AD NUMBER

ADB107745

LIMITATION CHANGES

TO:

Approved for public release; distribution is unlimited.

FROM:

Distribution authorized to U.S. Gov't. agencies only; Critical Technology; JAN 1986. Other requests shall be referred to Air Force Wright Aeronautical Laboratories, ATTN: FIBRA, Wright-Patterson AFB, OH 45433-6553.

AUTHORITY

D/A ltr dtd 1 Nov 1990

AFWAL-TR-86-3033

DESIGN, FABRICATION, TESTING AND ANALYSIS OF BOLTED STRUCTURAL ELEMENTS

R.L. Ramkumar
E.S. Saether
E. Tossavainen

Northrop Corporation, Aircraft Division
One Northrop Avenue
Hawthorne, California 90250

JULY 1986

Final Report for Period January 1984 thru December 1985

FLIGHT DYNAMICS LABORATORY
AIR FORCE WRIGHT AERONAUTICAL LABORATORIES
AIR FORCE SYSTEMS COMMAND
WRIGHT-PATTERSON AIR FORCE BASE, OHIO 45433-6553

NOTICE

When Government drawings, specifications, or other data are used for any purpose other than in connection with a definitely related Government procurement operation, the United States Government thereby incurs no responsibility nor any obligation whatsoever; and the fact that the government may have formulated, furnished, or in any way supplied the said drawings, specifications, or other data, is not to be regarded by implication or otherwise as in any manner licensing the holder or any other person or corporation, or conveying any rights or permission to manufacture use, or sell any patented invention that may in any way be related thereto.

This report has been reviewed by the Office of Public Affairs (ASD/PA) and is releasable to the National Technical Information Service (NTIS). At NTIS, it will be available to the general public, including foreign nations.

This technical report has been reviewed and is approved for publication.

VIPPERLA B. VENKAYYA
Project Engineer
Design & Analysis Methods Group

FREDERICK A. PICCHIONI, Lt Col, USAF
Chief, Analysis & Optimization Branch

FOR THE COMMANDER

ROGER J. HEGSTROM, Col, USAF
Chief, Structures & Dynamics Div.

"If your address has changed, if you wish to be removed from our mailing list, or if the addressee is no longer employed by your organization please notify AFWAL/FIBRA, W-PAFB, OH 45433-6553 to help us maintain a current mailing list".

Copies of this report should not be returned unless return is required by security considerations, contractual obligations, or notice on a specific document.

REPORT DOCUMENTATION PAGE

1a. REPORT SECURITY CLASSIFICATION UNCLASSIFIED	1b. RESTRICTIVE MARKINGS
2a. SECURITY CLASSIFICATION AUTHORITY	3. DISTRIBUTION/AVAILABILITY OF REPORT Distribution limited to U.S. Government Agencies only; critical technology; 1/86. Other requests must be referred to AFWAL/FIBRA, WPAB,OH 4543
2b. DECLASSIFICATION/DOWNGRADING SCHEDULE	
4. PERFORMING ORGANIZATION REPORT NUMBER(S) NOR 86-209	5. MONITORING ORGANIZATION REPORT NUMBER(S) AFWAL-TR-86-3033
6a. NAME OF PERFORMING ORGANIZATION Northrop Corporation Aircrart Division 6b. OFFICE SYMBOL (If applicable)	7a. NAME OF MONITORING ORGANIZATION Flight Dynamics Laboratory (AFWAL/FIBRA) Air Force Wright Aeronautical Laboratories
6c. ADDRESS (City, State and ZIP Code) One Northrop Avenue Hawthorne, CA 90250	7b. ADDRESS (City, State and ZIP Code) Wright-Patterson Air Force Base Dayton, Ohio 45433-6553
8a. NAME OF FUNDING/SPONSORING ORGANIZATION 8b. OFFICE SYMBOL (If applicable)	9. PROCUREMENT INSTRUMENT IDENTIFICATION NUMBER Contract F33615-82-C-3217
8c. ADDRESS (City, State and ZIP Code)	10. SOURCE OF FUNDING NOS.

PROGRAM ELEMENT NO.	PROJECT NO.	TASK NO.	WORK UNIT NO.
62201F	2401	02	55

11. TITLE (Include Security Classification) Design, Fabrication, testing and Analysis of Bolted Structural Elements

12. PERSONAL AUTHOR(S)
R. L. Ramkumar, E. S. Saether and E. Tossavainen

13a. TYPE OF REPORT	13b. TIME COVERED	14. DATE OF REPORT (Yr., Mo., Day)	15. PAGE COUNT
Final	FROM 1/1/84 TO 12/31/85	July 1986	63

16. SUPPLEMENTARY NOTATION

17. COSATI CODES			18. SUBJECT TERMS (Continue on reverse if necessary and identify by block number)
FIELD	GROUP	SUB. GR.	Bolted structural element, graphite/epoxy skins, composite-to-metal joint, design, analysis, testing, failure records, correlation studies
01	03		
13	05		

19. ABSTRACT (Continue on reverse if necessary and identify by block number)

This report presents design and fabrication details for a bolted structural element concept that was studied as a potential alternative to the existing vertical tail-to-fuselage attachment in the F/A-18A aircraft. Two elements were fabricated, based on an approximate and conservative preliminary design, and were subjected to two lifetimes of representative tension-dominated F/A-18A vertical tail spectrum loading. Both elements survived the fatigue loads with no indication of failure. Their residual tensile failure loads were approximately 30% larger than the design ultimate load value. The elements were also analyzed using the SAMCJ computer code developed in this Northrop/AFWAL program. Analytically predicted element strength was within 7% of the measured value. Analytically predicted failure location also coincided with experimental observations. However, the observed failure mode could not be predicted by the developed analysis. Nevertheless, this task established the adequacy of the SAMCJ computer code for predicting the strength of bolted joints in composite structures.

20. DISTRIBUTION/AVAILABILITY OF ABSTRACT	21. ABSTRACT SECURITY CLASSIFICATION
UNCLASSIFIED/UNLIMITED ☐ SAME AS RPT. ☒ DTIC USERS ☐	Unclassified

22a. NAME OF RESPONSIBLE INDIVIDUAL	22b. TELEPHONE NUMBER (Include Area Code)	22c. OFFICE SYMBOL
V. B. Venkayya	(513) 255-6992	AFWAL/FIBRA

DD FORM 1473, 83 APR EDITION OF 1 JAN 73 IS OBSOLETE.

PREFACE

This report was prepared under Contract F33615-82-C-3217, titled "Bolted Joints in Composite Structures: Design, Analysis and Verification," and administered by the Air Force Wright Aeronautical Laboratories. Dr. V. B. Venkayya was the Air Force project engineer, and was assisted by Capt. M. Sobota and Lt. D. L. Graves as program co-monitors. The program manager and principal investigator at Northrop was Dr. R. L. Ramkumar.

This report provides details of the design, fabrication, testing and analysis efforts conducted under Task 3 in the referenced program (Project 2401).

The authors gratefully acknowledge the support provided by the following personnel:

Preliminary Design	H. Zamani, S. Averill
Element Fabrication	W. Spore, F. Uldrich
Testing	A. McQuillian, P. Dager
Graphics	R. Cordero
Typing	C. Harris

TABLE OF CONTENTS

SECTION		PAGE
1	INTRODUCTION	1
2	DESIGN AND FABRICATION OF TASK 3 ELEMENTS	3
	2.1 Background	3
	2.2 Design of Task 3 Elements	9
	2.3 Fabrication of Task 3 Elements	10
3	TASK 3 ELEMENT TEST RESULTS	23
	3.1 Task 3 Element Test Procedure	23
	3.2 Task 3 Element Test Results	30
4	ANALYSIS OF TASK 3 ELEMENT	53
5	CONCLUSIONS	61
REFERENCES		63

LIST OF ILLUSTRATIONS

Figure		Page
1	Parts of the Bolted Element Tested in Reference 7	5
2	An Assembeled Bolted Element Tested in Reference 7	6
3	Typical Net Section Failure of the Aluminum Root Rib, Observed in Reference 7, Under Static Tension Loading	7
4	Net Section Failure in the Aluminum Tab Region, Observed in Reference 7, During Residual Tension Strength Testing of the Thin-Tab Element	8
5	Fabrication Drawing for the Element Spar	11
6	Fabrication Drawing for the Element Root Rib	13
7	Fabrication Drawing for the Element Skins	15
8	Fabrication Drawing for the Element Assembly	17
9	Photomicrographs of Cross-Sections of the 59-Ply and 41-Ply Locations in the Graphite/Epoxy Skin	19
10	Photograph of an Assembled Task 3 Element	20
11	Tab Thickness Measurements on Element 1	21
12	Tab Thickness Measurements on Element 2	22
13	Strain Gage Locations in Element 1 Tabs	24
14	Strain Gage Locations in Element 2 Tabs	25
15	Close-Up of Tab 1 of Element 1 Showing the Strain Gage Arrangement	26
16	Photograph of Assembled Element in the Test Machine, Prior to Loading	27
17	Spectral Density Functions Associated with the Tension-Dominated Spectrum Loading Imposed on Task 3 Elements	28

LIST OF ILLUSTRATIONS (CONCLUDED)

Figure		Page
18	Exceedance Counts on Peaks, Valleys and Amplitudes in the Imposed Spectrum Loading.....	29
19	Hysteresis Curves for Element 1 After 0, 1 and 2 Lifetimes of Spectrum Loading.....	31
20	Failed Tab 2 in Element 1.....	32
21	Failed Tab 1 in Element 1 After Reloading.....	33
22	Strain Gage and Clip Gage Reading from Element 1 (See Figure 13).....	36
23	Strain Variations with Imposed Load for Element 1.....	37
24	Summary of Strains at Failure for Element 1.....	41
25	Hysteresis Curves for Element 2 After 0, 1 and 2 Lifetimes of Spectrum Loading.....	42
26	Failed Element 2 Tabs.....	43
27	Progression of Element 2 Failure During Reloading.....	44
28	Strain Gage and Clip Gage Readings from Element 2 (See Figure 14).....	46
29	Strain Variations with Imposed Load for Element 2.....	47
30	Summary of Strains at Failure for Element 2.....	51
31	Dimensions of the Critical Skin Tab and the Fuselage Attachment Frame.....	54
32	Load Distribution Among Fasteners, Failure Location and Failure Mode in the Graphite/ Epoxy Tabs.....	56
33	Analytically Predicted Element Load Levels to Precipitate Net Section, Bearing and Shear-out Modes of Tab Failure at Each Fastener Location.....	59

SECTION 1

INTRODUCTION

This report summarizes Task 3 accomplishments on the ongoing Northrop/AFWAL program titled "Bolted Joints in Composite Structures: Design, Analysis and Verification." This program was initiated with the following objectives: (a) to develop analytical methods for strength and life prediction of bolted joints, accounting for stress concentration interactions, if any; (b) to verify the developed analyses through a series of experiments; and (c) to develop a comprehensive, design-oriented guide for bolted joints in composite structures.

To achieve program objectives four tasks were identified. Under Task 1, analytical techniques were developed for the prediction of the strength of single fastener joints in composite structures, accounting for finite joint geometry effects and localized through-the-thickness strain variation (Reference 1). The developed analyses were complemented and validated by testing 450 single-fastener composite-to-metal joint specimens of various configurations (Reference 2).

Under Task 2, analytical techniques were developed to predict the strength of multiple fastener joints in composite structures accounting for stress concentration interaction effects, if any (Reference 3). The developed analyses were validated by conducting 159 static tests on multifastener specimens with different fastener arrangements, and in selected cases, with circular cutouts adjacent to the fasteners (Reference 4).

Task 3 was defined to ensure that the methodology developed under Tasks 1 and 2 can be used to design and analyze full-scale bolted structural components. Task 3 tests were conducted on elements representative of a typical bolted vertical stabilizer root section. The test element was analyzed using the methodology developed in Task 2, and theoretical predictions correlated well with experimental results.

In Task 4, results from Tasks 1 to 3, and available information from previous investigations, were compiled to develop a guide for the design of bolted composite structures (Reference 5). The guide includes general design guidelines, easy-to-use design curves, and detailed instructions, with examples, for the use of the developed computer programs in designing bolted composite structures.

In the following sections, the design, fabrication, testing and analysis of Task 3 bolted structural elements is discussed.

SECTION 2

DESIGN AND FABRICATION OF TASK 3 ELEMENTS

2.1 Background

In Reference 6, a composite-to-metal bolted joint design was assessed as an alternative to a high load transfer composite-to-titanium, step lap, adhesively bonded joint. The existing production tail structure of the F/A-18A was used as the baseline for this assessment. In Reference 7, the conceptual bolted joint selected in Reference 6 was evaluated further and refined, based on test results that accounted for environmental effects, production and service-induced flaws, etc. This effort included tests on many coupons and nineteen larger elements.

The design of the elements tested in Reference 7 was based on F/A-18A design conditions and their associated loads. Swept torsion and swept moment at the root, caused by differential pressure acting on the tail surface under various design conditions, were used to compute chordwise and spanwise loads (Reference 8). Based on these results, the 22-percent spar was reaffirmed to be the location of maximum spanwise load transfer. The spanwise thermal load reactions at or near the root joint contributed between 1 and 1.5 kip/in of the total 7 kip/in peak reaction. The critical design condition induced shear flows and chordwise loads that were much smaller than the spanwise loads, except in one skin location just forward of the 62.5-percent spar. There, Nx (spansiwe) was 4115 lb/in, Ny (chordwise) was 628 lb/in, and Nxy or q (shear flow) was approximately 1000 lb/in. The selected element design was verified to be adequate under this biaxial loading condition, and also accounted for the chordwise load due to the thermal mismatch between the graphite/epoxy skin and the aluminum closeout rib.

The bolted joint element tested in Reference 7 was made up of a forged 7075-T736 aluminum root rib (with a web, flanges and tabs), and two AS4/3501-6 graphite/epoxy skins (See Figure 1). The graphite/epoxy skins contained 41 plies in a 49/39/12 (percentages of 0 degrees, + or - 45-degrees and 90-degree plies, respectively, with the zero-degree direction aligned with the loading direction) layup. At the graphite/epoxy-to-root rib joint, 5/16-inch-diameter high-strength steel fasteners were used. An assembled element is shown in Figure 2.

Static tension tests on the element in Figure 2 resulted in a net section failure of the aluminum root rib, across the first row of bolts (Figure 3). The same failure resulted when the element was subjected to a residual static tension test after completing two lifetimes of a tensin-dominated spectrum fatigue loading. Under a static compression load, however, the laterally constrained graphite/epoxy skin suffered a pure compressive failure on the blind side, directly above the second row of bolts. The same failure resulted when the element was subjected to a residual static compression test after completing two lifetimes of a compression-dominated spectrum fatigue loading.

An element with a thinner tab segment was also tested under static tension, after it was subjected to a tension-dominated spectrum fatigue loading. In this case, a net section failure occurred in the tab region of the root rib, across the upper row of bolts that connect it to the fuselage stub frame (see Figure 4). A fractographic analysis of the tab revealed fatigue-induced cracks around the two hole boundaries. Also, multiple fatigue crack initiation sites were identified in the fillet region of the tab.

In summary, the element tests in Reference 7 indicated that the aluminum root rib and the support fitting were more

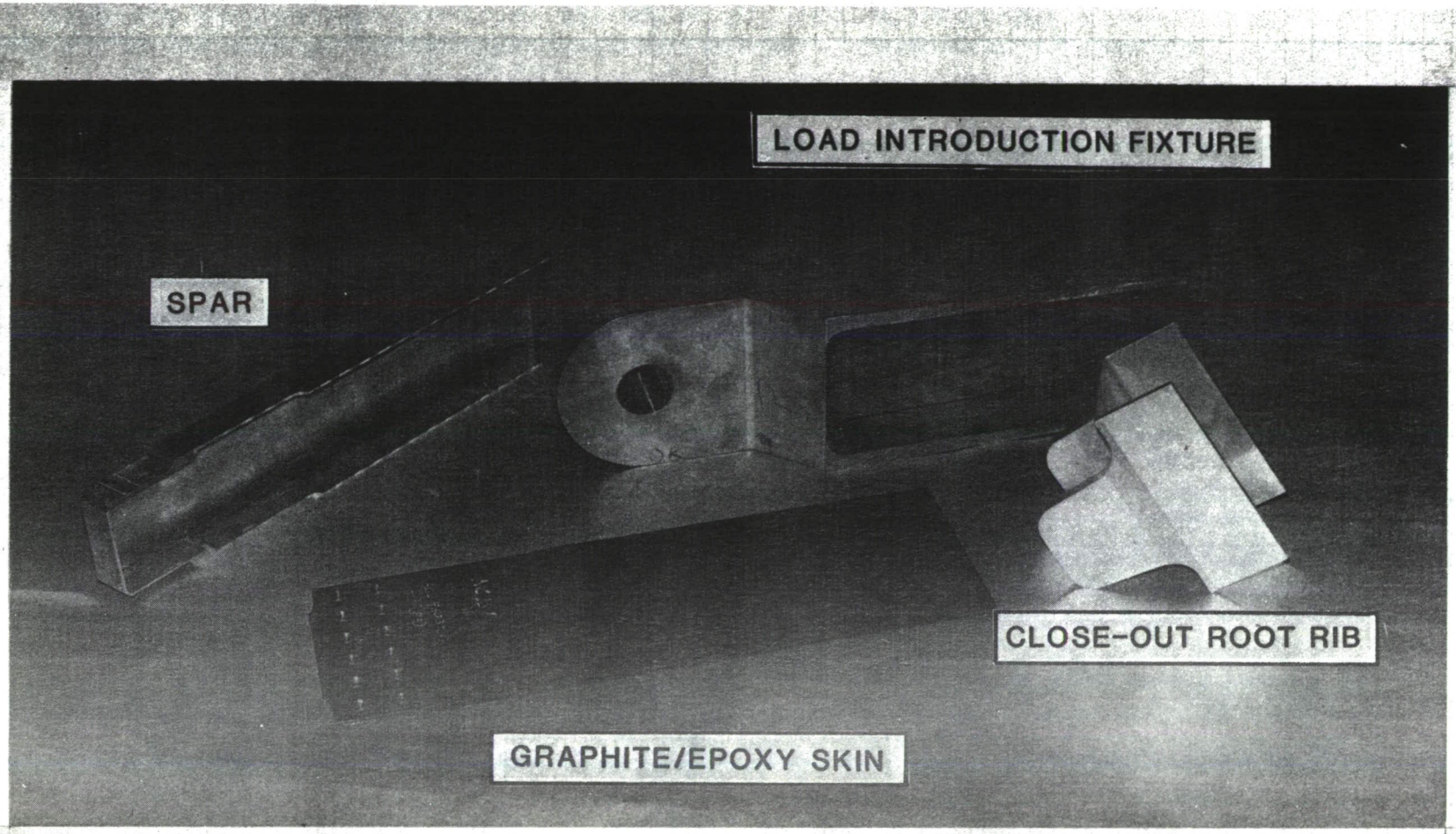

Figure 1. Parts of the Bolted Element Tested in Reference 7.

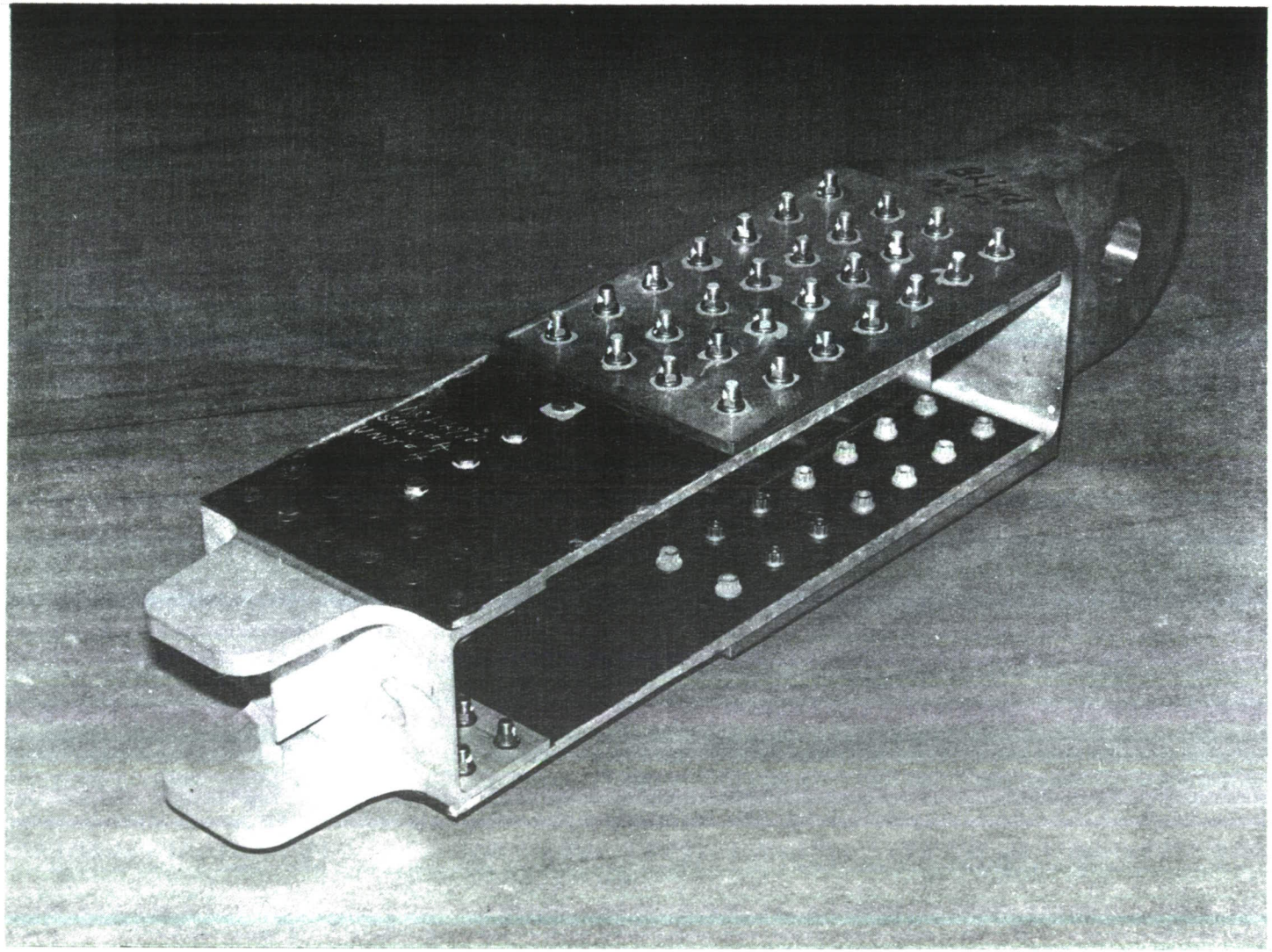

Figure 2. An Assembled Bolted Element Tested in Reference 7.

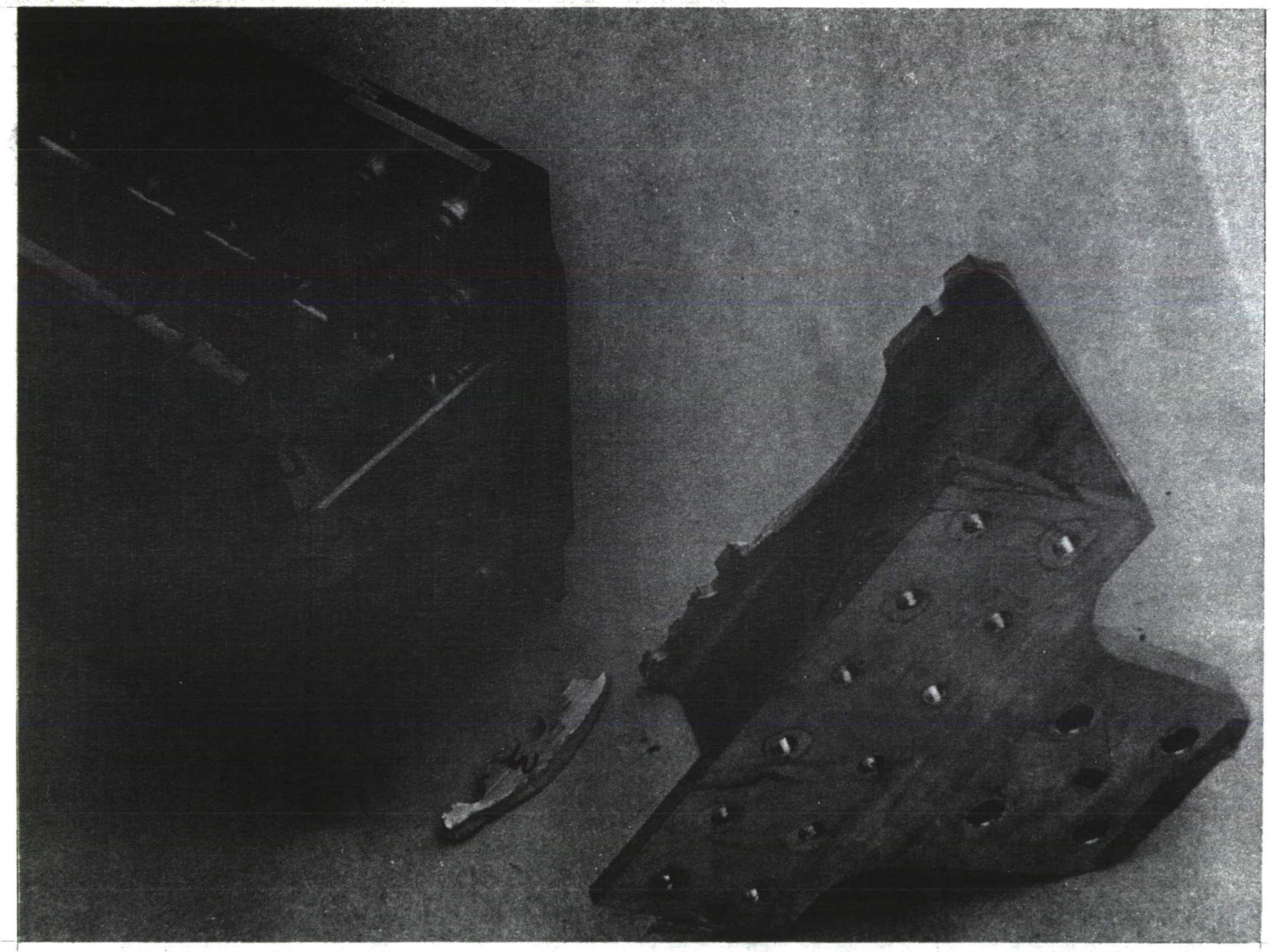

Figure 3. Typical Net Section Failure of the Aluminum Root Rib, Observed in Reference 7, Under Static Tension Loading.

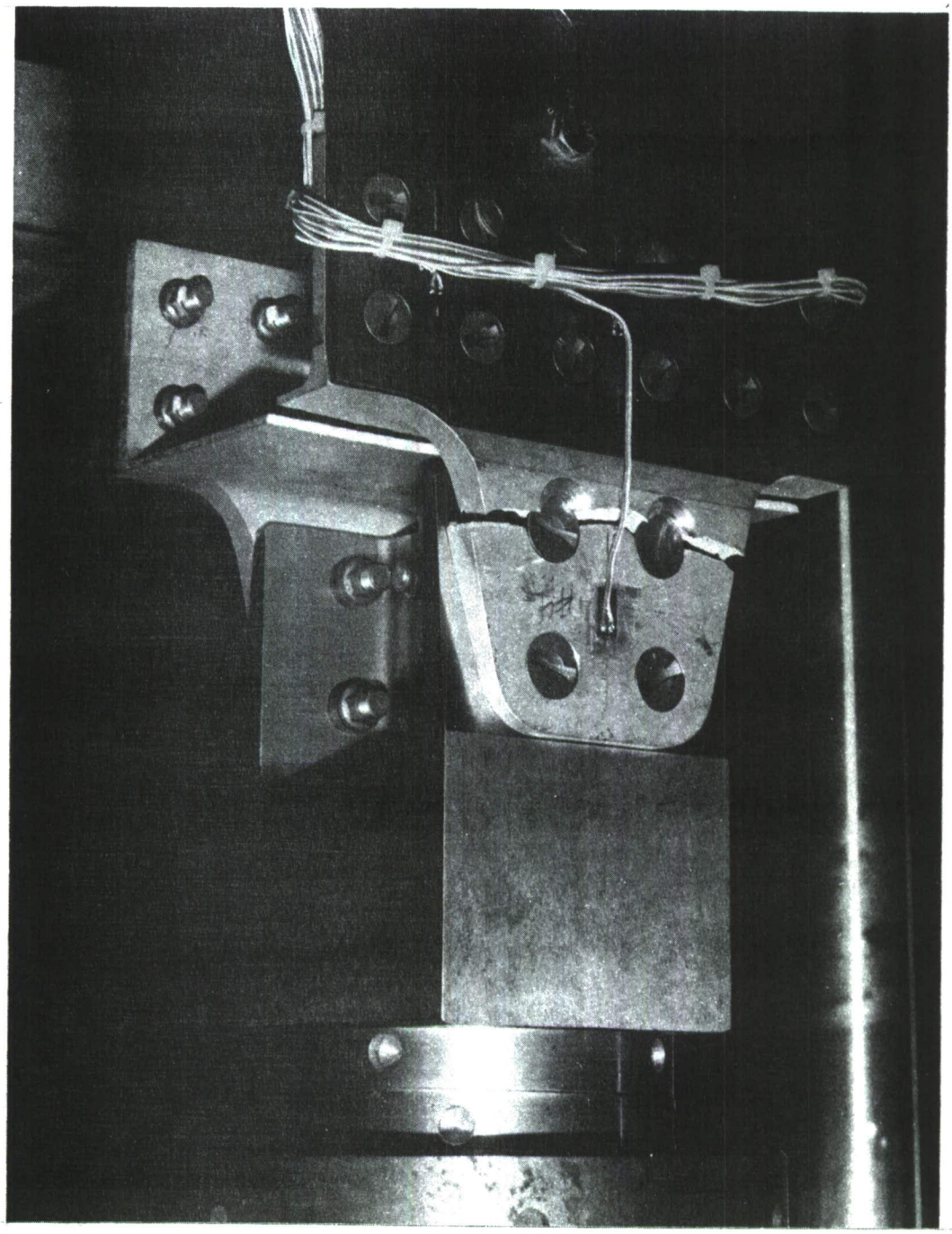

Figure 4. Net Section Failure in the Aluminum Tab Region, Observed in Reference 7, During Residual Tension Strength Testing of the Thin-Tab Element.

susceptible to static and fatigue failure under tension than the graphite/epoxy skins. It was, therefore, realized than an element design change was necessary before applying the results from Reference 7 to the design of an efficient subcomponent. This task was successfully accomplished in this Northrop/AFWAL program and proved to be valuable in designing and fabricating subcomponents in the Northrop/NADC program. The changes incorporated in the Northrop/AFWAL element included a lightly loaded root rib and the direct attachment of extended graphite/epoxy skins to the fuselage fittings. The following sub-sections describe the design and fabrication details of the elements tested in this Northrop/AFWAL program.

2.2 Design of Task 3 Elements

The initial design of the Task 3 bolted element was based on the approximate analysis used in Reference 7 and the test results generated in References 6 and 7. The analysis assumed that the load transferred by the two rows of bolts in the graphite/epoxy tab bear a maximum ratio of 1.5 to 1. The adequacy of the tab layup and the fasteners to transfer the design ultimate load of 70.2 kips was verified using the analysis developed in Reference 9. The design ultimate load was obtained from the F/A-18A empennage stress analysis report (Reference 8).

The Task 3 element tested in this Northrop/AFWAL program is an improvement over those tested in Reference 7. The direct attachment of the graphite/epoxy skins to the fuselage frame eliminates the need for an attaching root rib, saving weight and reducing machining costs. This also precludes the fatigue failure that occurred in the tab region of the aluminum root rib in Reference 7. However, the direct attachment of the skins to the stub frame introduces a higher running load in the graphite/epoxy tab region. A preliminary analysis of this element indicated that the 41-ply skin has to be increased to a

60-ply layup in the tab region. The graphite/epoxy tab could be later machined to fit the attachment fittings used in Reference 7. The analysis also indicates that 3/8-inch-diameter, high-strength (125 ksi in shear) steel bolts should be used at the graphite skin-to-stub frame joint.

2.3 Fabrication of Task 3 Elements

Fabrication drawings for the spar, rib and the graphite/ epoxy skins of the Task 3 element are presented in Figures 5 to 7, respectively. Figure 8 presents an assembly drawing for the bolted element. The spar was fabricated using 7075-T7351 aluminum alloy, and the rib was fabricated using 7050-T73651 (or 7050-T7451) aluminum. Graphite/epoxy skins were fabricated using AS4/3501-6 prepreg in accordance with established process procedures (NAI-1460). Inspection tests on the prepreg yielded a resin content of 33.8% by weight, a fiber areal weight of 148 gm/m , and 0.6 % of volatiles. Process control tests on the fabricated skins yielded a resin content of 23.9% by weight, a fiber volume of 69%, a laminate specific gravity of 1.62, a void content of less than 0.1% by volume, and a cured ply thickness of 0.0049 inch.

Two elements were fabricated and assembled in accordance with Figures 5 to 8. Photomicrographs of cross-sections of 59-ply and 41-ply locations in the graphite/epoxy are presented in Figure 9. These records verify the presence of the design layup at these skin locations. Figure 10 presents a photograph of an assembled Task 3 element.

Figures 11 and 12 present the tab thickness measurements at various locations in the two skins of each element. Figure 11 indicates that one tab in element 1 was machined to be approximately 5 plies thinner than the other tab. Figure 12 indicates that the two skins in element 2 were machined to be the same thicknesses.

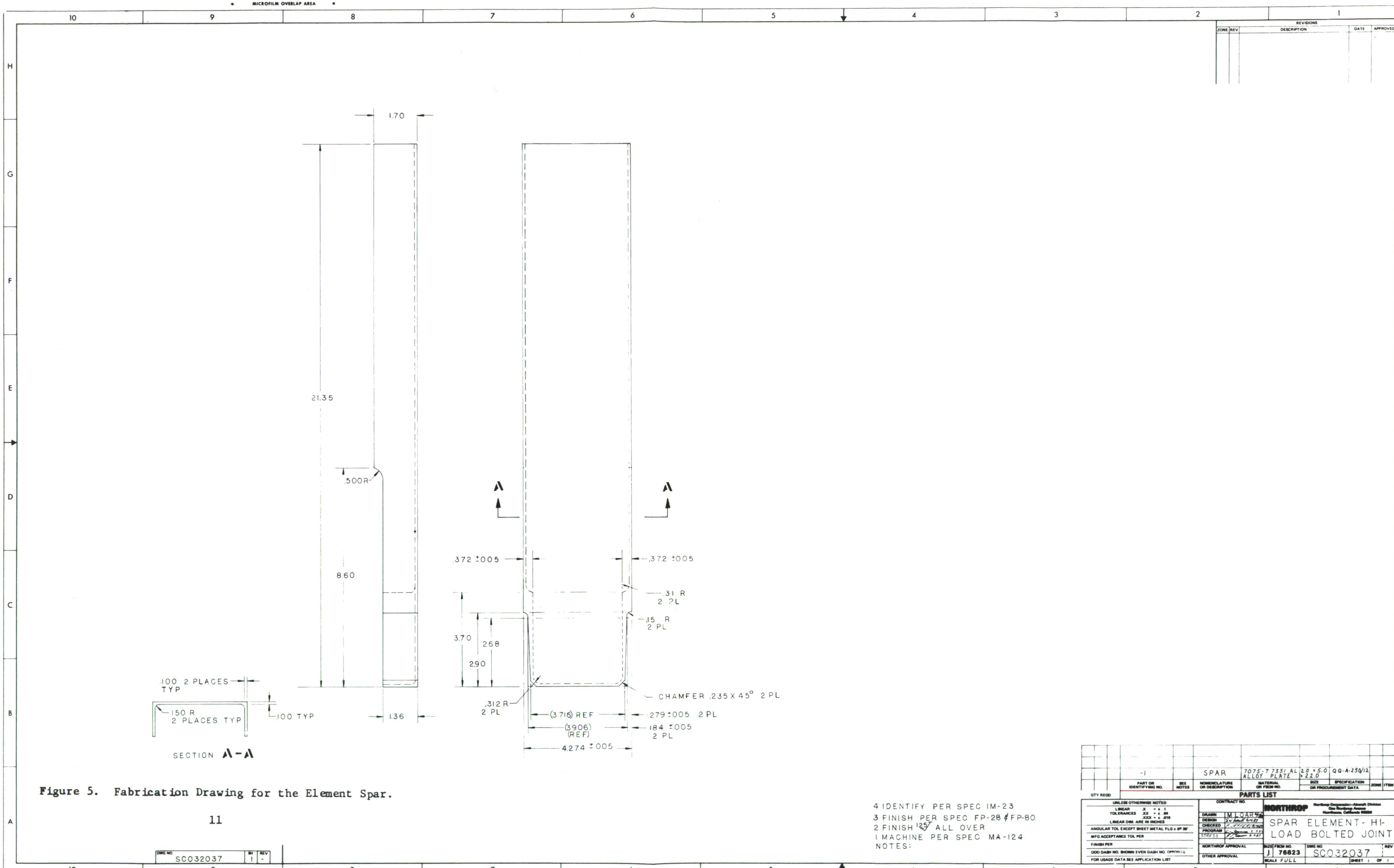

Figure 5. Fabrication Drawing for the Element Spar.

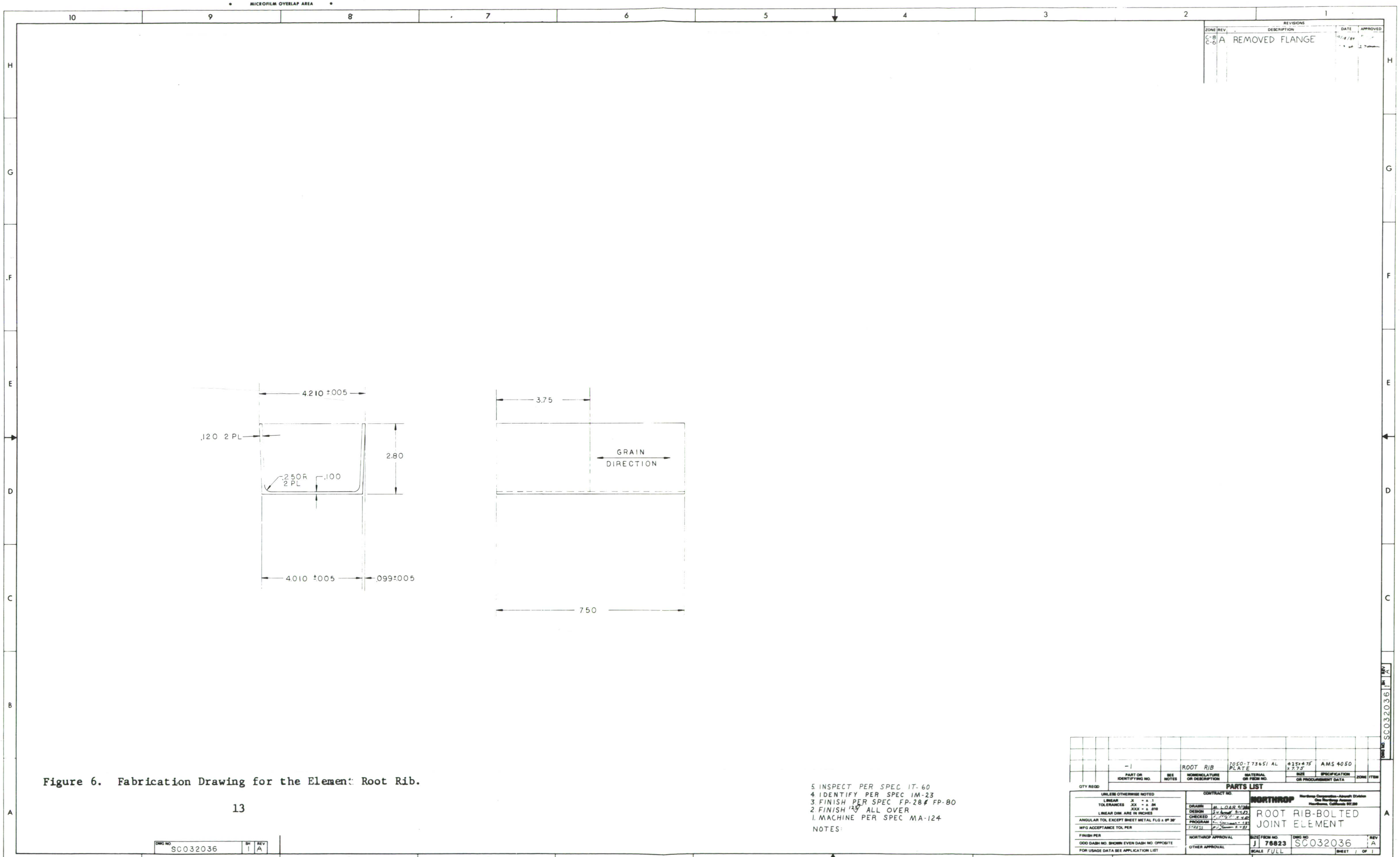

Figure 6. Fabrication Drawing for the Element: Root Rib.

STACKING SEQUENCE	
PLY NO.	ORIENTATION
P0	0° 120 WEAVE GLASS CLOTH
P1	+ 45°
P2	- 45°
P3	0°
P4	0°
P5	90°
P6	0°
P7	0°
P8	+ 45°
P9	- 45°
P10	0°
P11	0°
P12	+ 45°
P13	- 45°
P14	0°
P15	0°
P16	90°
P17	0°
P18	0°
P19	+ 45°
P20	- 45°
P21	0°
P22	90°
P23	0°
P24	+ 45°
P25	- 45°
P26	0°
P27	0°
P28	+ 45°
P29	- 45°
P30	90°
P31	- 45°
P32	+ 45°
P33	0°
P34	0°
P35	- 45°
P36	+ 45°
P37	0°
P38	90°
P39	0°
P40	- 45°
P41	+ 45°
P42	0°
P43	0°
P44	90°
P45	0°
P46	0°
P47	- 45°
P48	+ 45°
P49	0°
P50	0°
P51	- 45°
P52	+ 45°
P53	0°
P54	0°
P55	90°
P56	0°
P57	0°
P58	- 45°
P59	+ 45°
P60	0° 120 WEAVE GLASS CLOTH

Figure 7. Fabrication Drawing for the Element Skins.

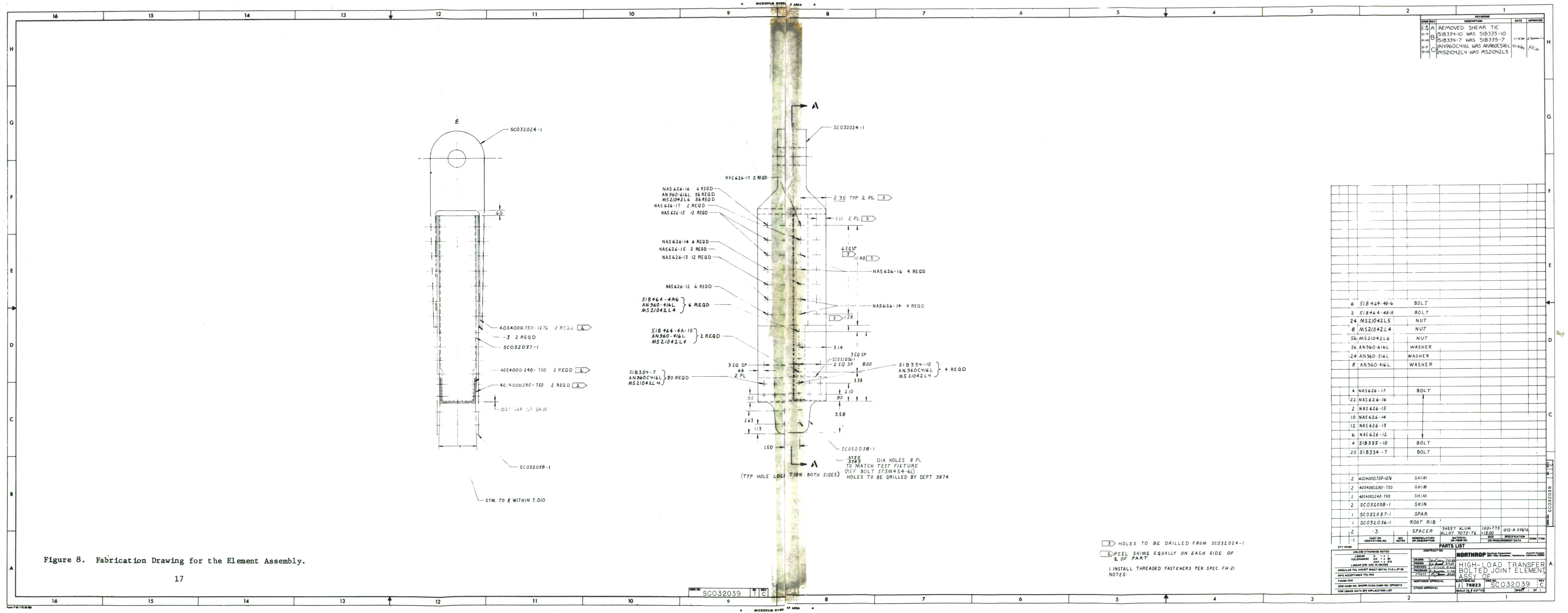

Figure 8. Fabrication Drawing for the Element Assembly.

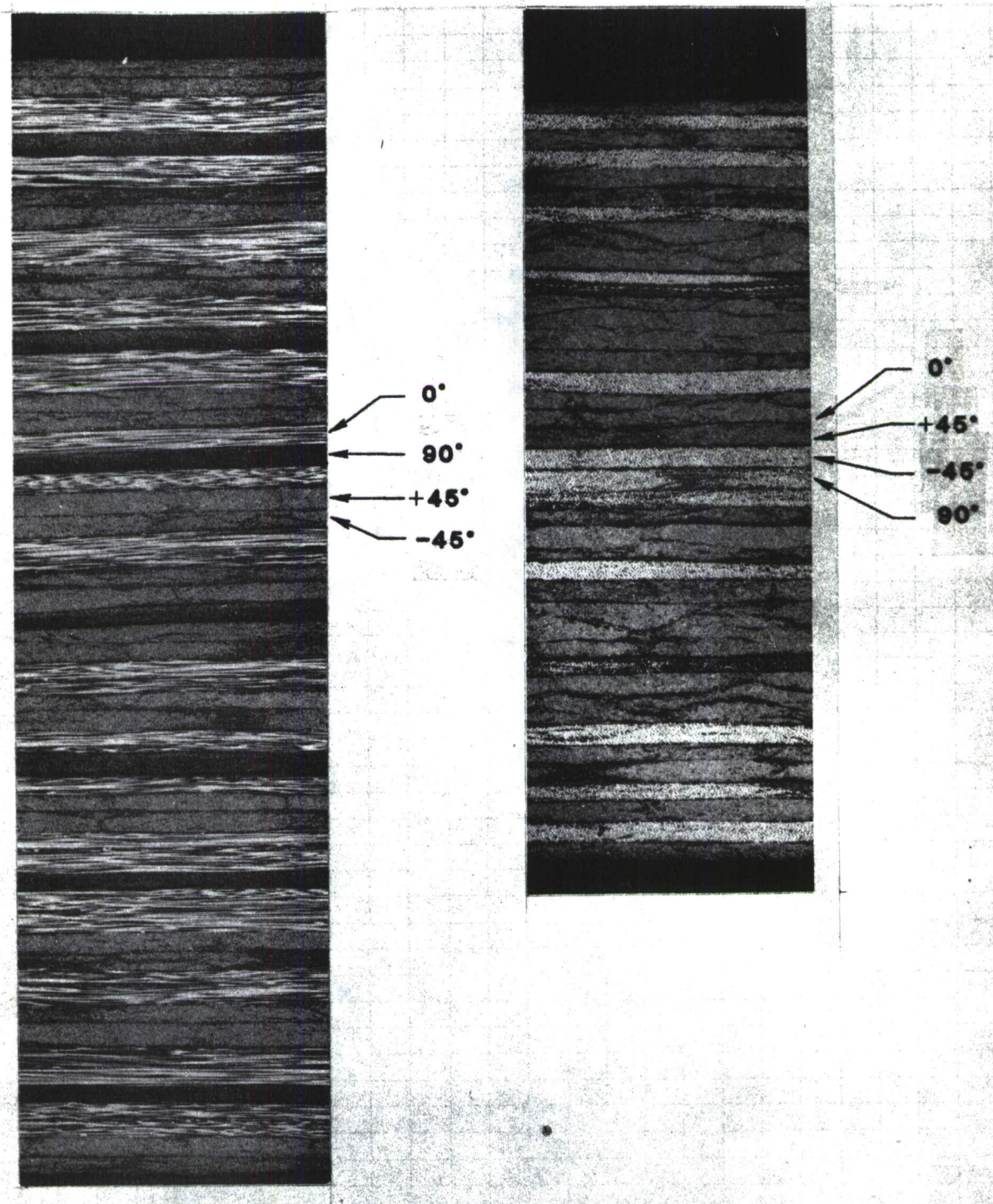

Figure 9. Photomicrographs of Cross-Sections of the 59-Ply and 41-Ply Locations in the Graphite/Epoxy Skin.

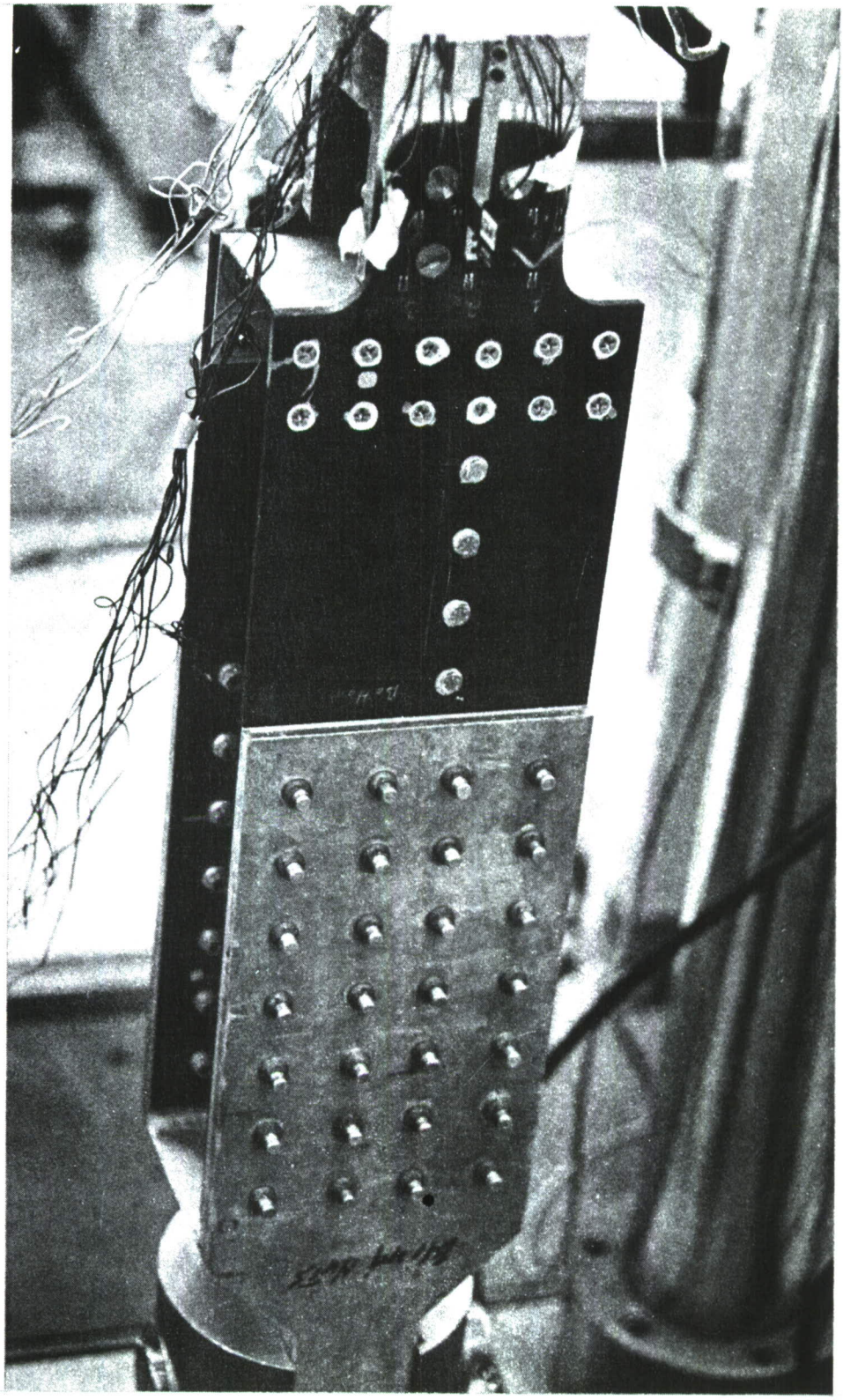

Figure 10. Photograph of an Assembled Task 3 Element.

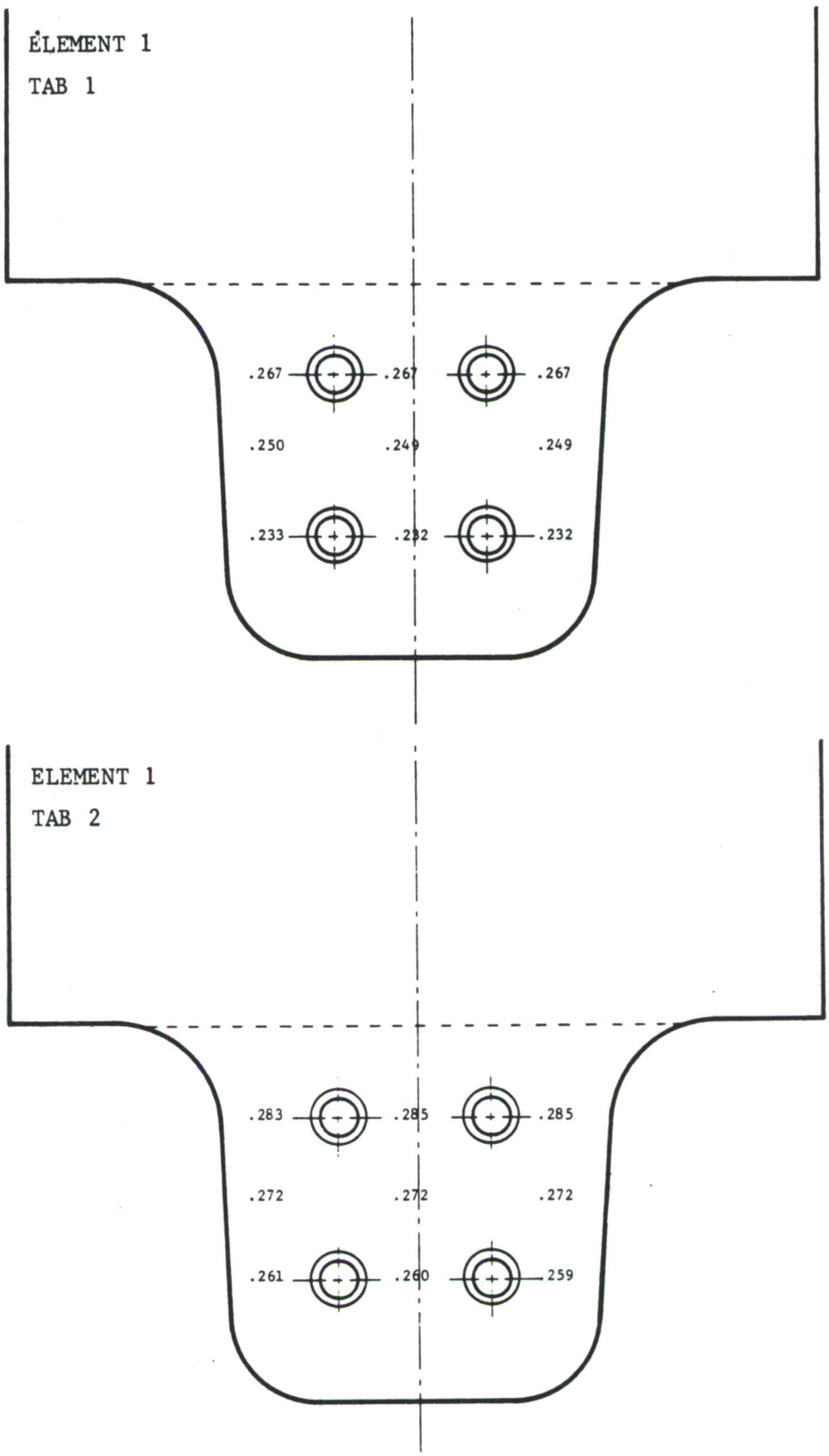

Figure 11. Tab Thickness Measurements on Element 1.

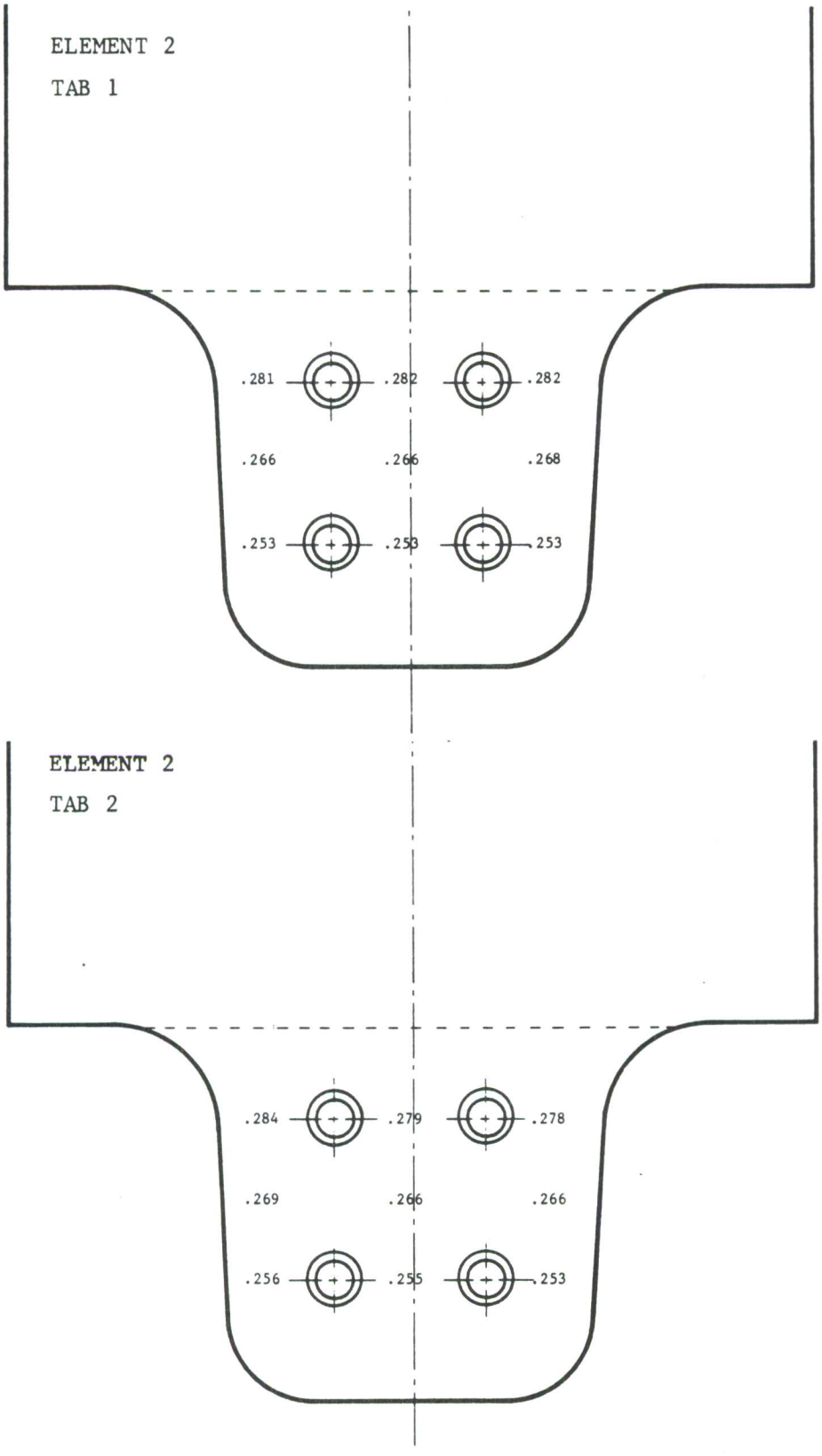

Figure 12. Tab Thickness Measurements on Element 2.

SECTION 3

TASK 3 ELEMENT TEST RESULTS

Task 3 elements were initially subjected to two lifetimes of a tension-dominated spectrum fatigue loading, and subsequently tested under static tension to obtain their residual tensile strengths. The following sub-sections describe the employed test procedure and test results.

3.1 Task 3 Element Test Procedure

Prior to testing, axial strain gages were bonded to the graphite/epoxy tabs at the locations shown in Figures 13 and 14. Figure 15 shows a close-up of tab 1 of element 1, indicating the strain gage arrangement on this surface. A photograph of an assembled element in the test machine, prior to load introduction, is shown in Figure 16.

The two elements were initially subjected to two lifetimes of a representative tension-dominated F/A-18A vertical tail spectrum loading, under ambient environmental conditions. Figure 17 presents the spectral density functions associated with the imposed loading. The exceedance counts on the peaks, valleys and amplitudes in the spectrum are plotted in Figure 18. The maximum spectrum load was the design limit load (46.8 kips) for the first lifetime, and the design ultimate load (70.2 kips) for the second lifetime. The imposed spectrum load was significantly more severe than the actual F/A-18 vertical tail design spectrum load. Elements 1 and 2 survived the imposed spectrum loading with no indication of local or total fatigue failure.

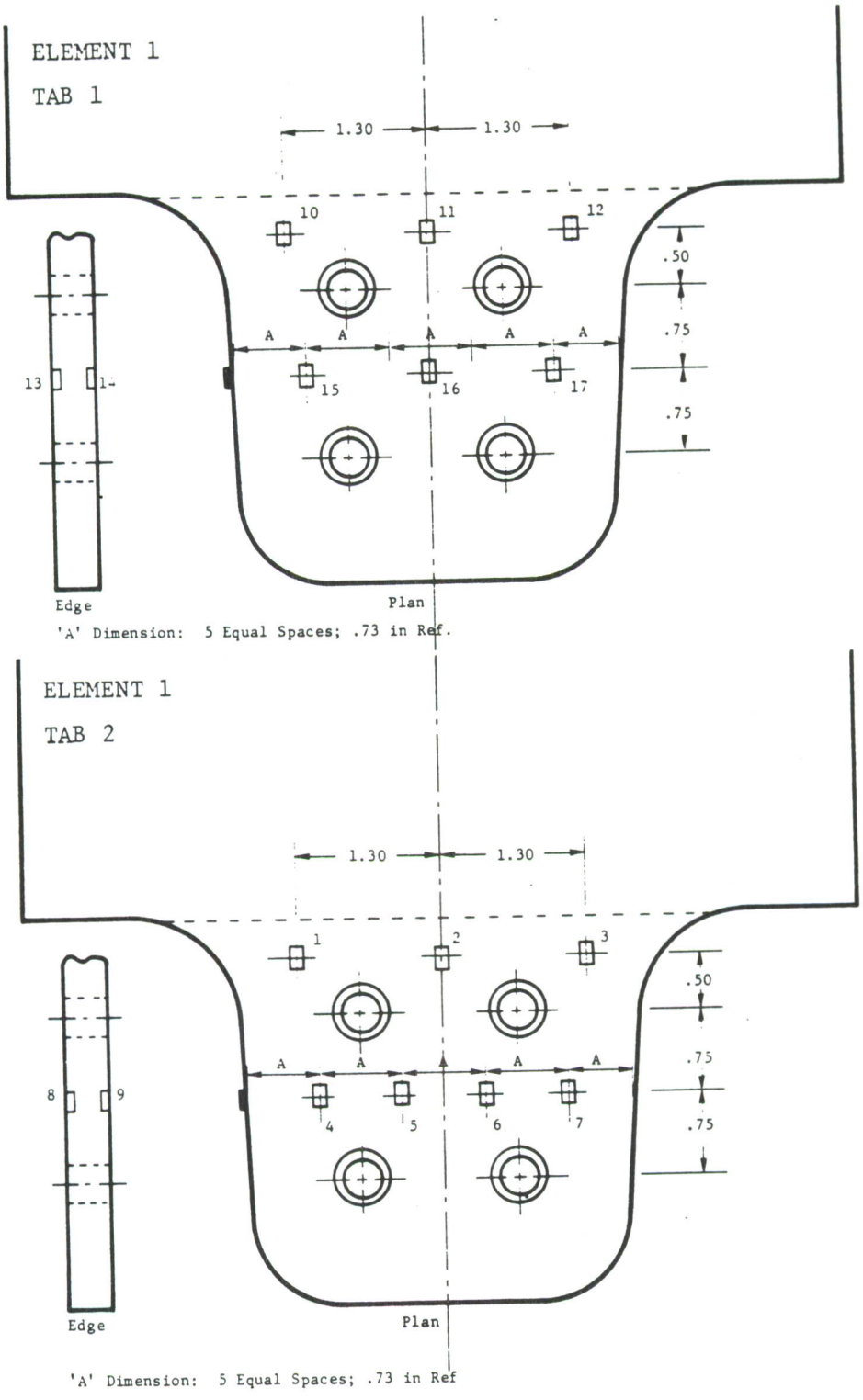

Figure 13. Strain Gage Locations in Element 1 Tabs.

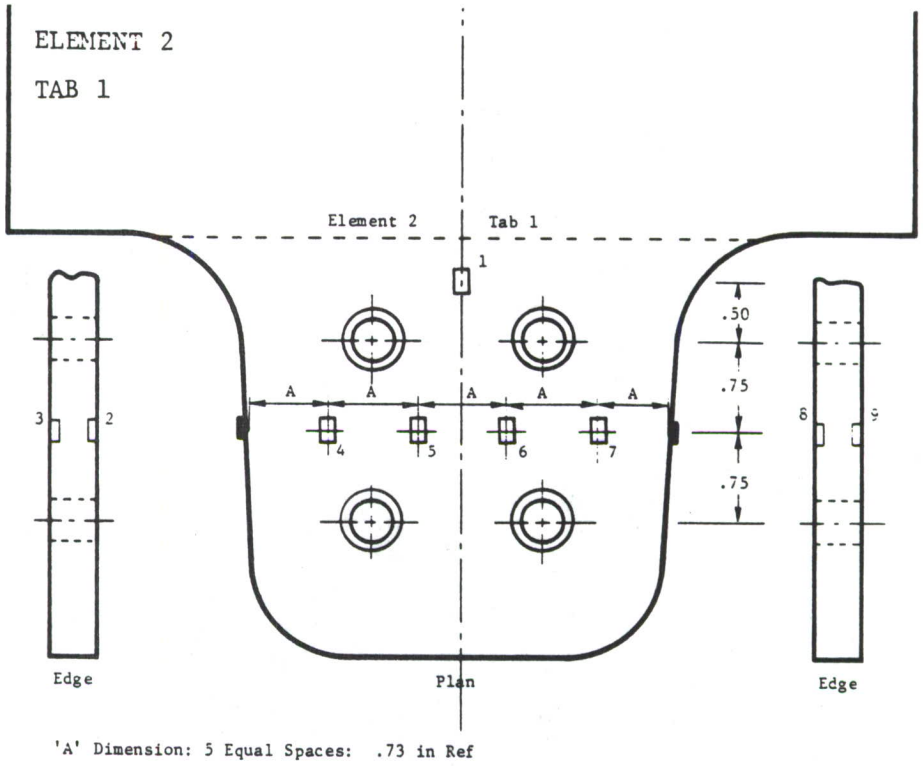

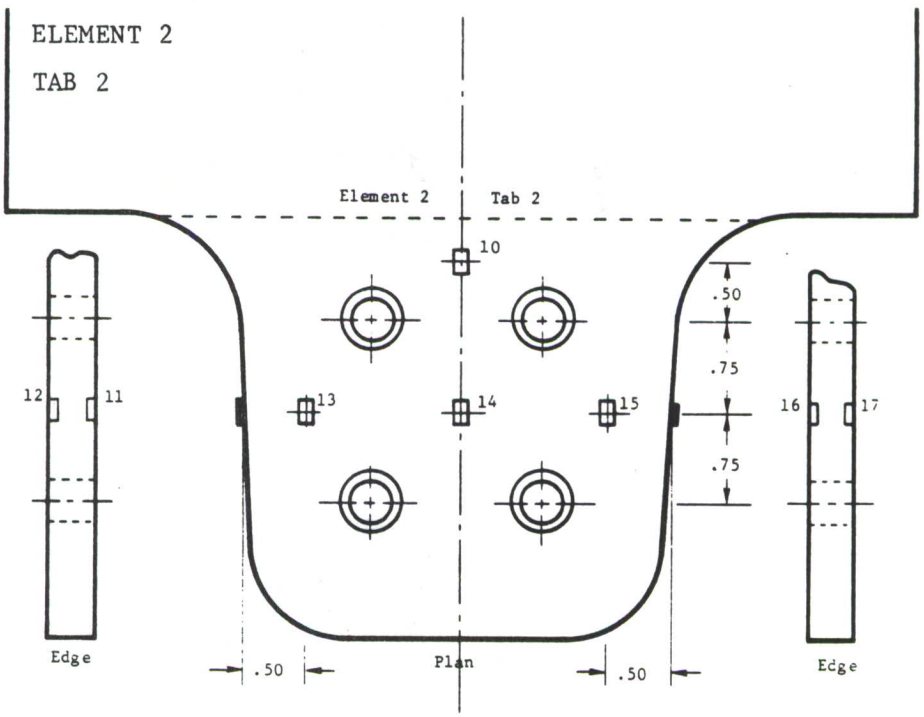

Figure 14. Strain Gage Locations in Element 2 Tabs.

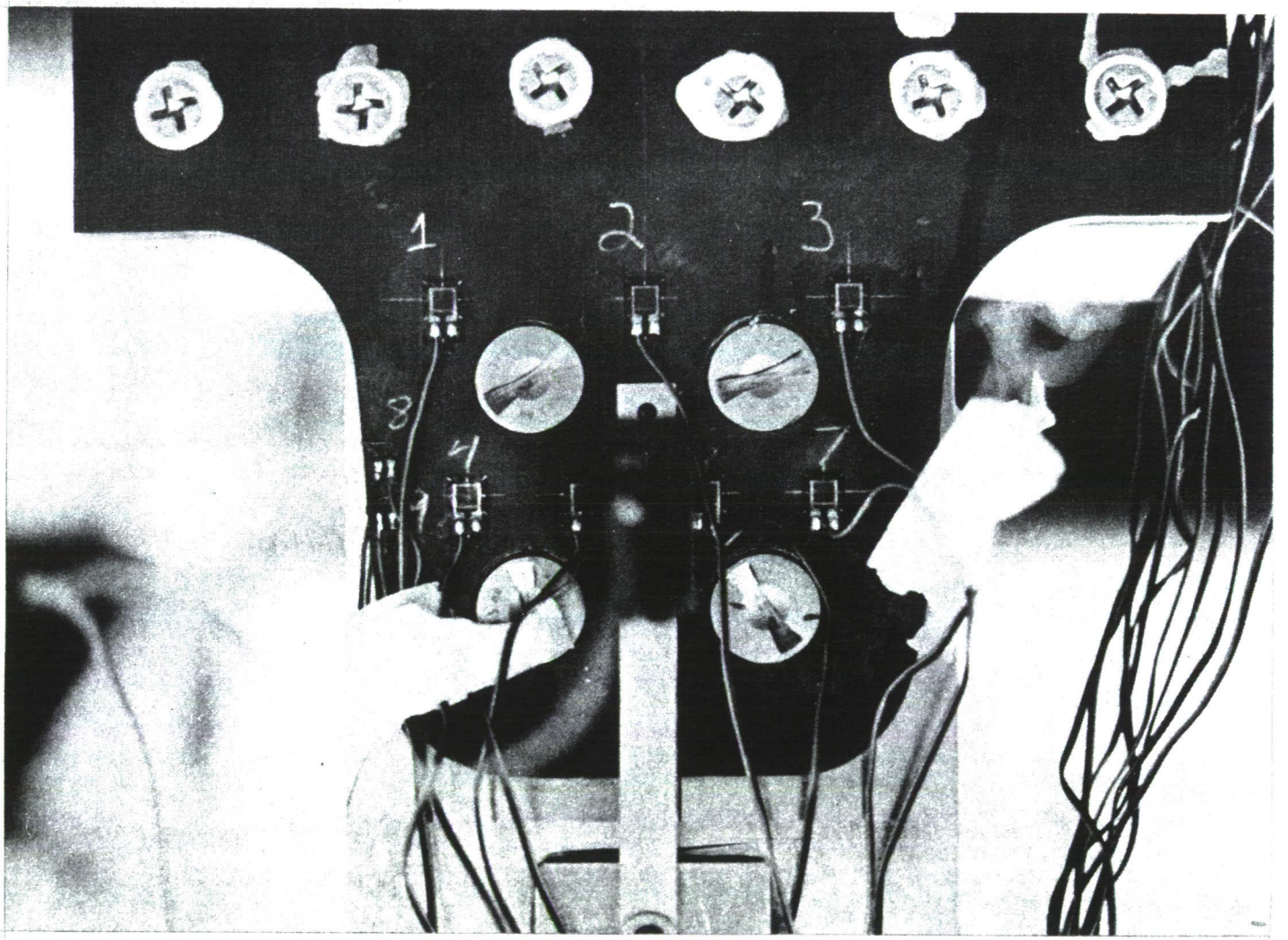

Figure 15. Close-Up of Tab 1 of Element 1 Showing the Strain Gage Arrangement.

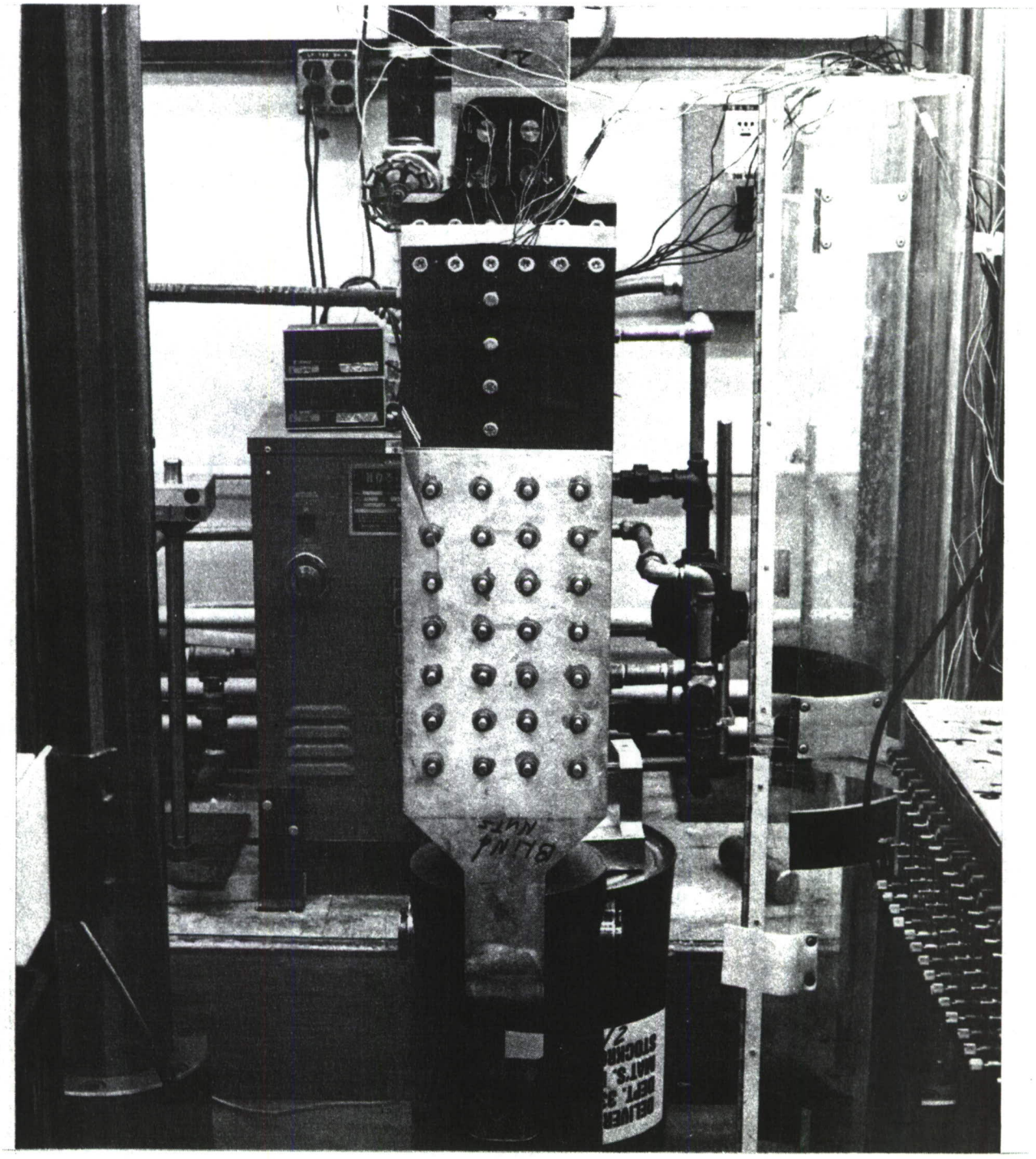

Figure 16. Photograph of an Assembled Element in the Test Machine, Prior to Loading.

**** SPECTRAL DENSITY FUNCTIONS ****

SERIAL # MBJV81 F18VS.D

DATE 11-FEB-83 TIME 9:24:56

# OF EVENTS	PEAKS	VALLEYS	AMPLITUDES	MEAN LEVELS
**** X = 100	1	0	0	0
100 > X >= 95	44	0	0	0
95 > X >= 90	20	0	0	0
90 > X >= 85	30	0	0	0
85 > X >= 80	2	0	0	1
80 > X >= 75	5	0	0	54
75 > X >= 70	96	0	0	31
70 > X >= 65	164	2	0	45
65 > X >= 60	39	0	0	277
60 > X >= 55	62	102	0	277
55 > X >= 50	44	135	0	94
50 > X >= 45	205	67	9	20
45 > X >= 40	36	35	9	86
40 > X >= 35	98	11	30	274
35 > X >= 30	270	95	110	215
30 > X >= 25	31	81	111	148
25 > X >= 20	5	96	190	96
20 > X >= 15	6	47	556	470
15 > X >= 10	1089	24	958	215
10 > X >= 5	1935	236	3735	1777
5 > X >= 0	388	1391	3509	3841
0 > X >= -5	36	1143	0	1118
-5 > X >= -10	3	794	0	162
-10 > X >= -15	0	263	0	16
-15 > X >= -20	0	63	0	0
-20 > X >= -25	0	16	0	0
-25 > X >= -30	0	5	0	0
-30 > X >= -35	0	2	0	0
-35 > X >= -40	0	0	0	0
-40 > X >= -45	0	0	0	0
-45 > X >= -50	0	0	0	0
-50 > X >= -55	0	0	0	0
-55 > X >= -60	0	0	0	0
-60 > X >= -65	0	0	0	0
-65 > X >= -70	0	0	0	0
-70 > X >= -75	0	0	0	0
-75 > X >= -80	0	0	0	0
-80 > X >= -85	0	0	0	0
-85 > X >= -90	0	0	0	0
-90 > X >= -95	0	0	0	0
-95 > X >= -100	0	0	0	0
**** X = -100	0	0	0	0
TOTALS	4609	4608	9217	9217

*** # OF POINTS PROCESSED = 9222 ***

Figure 17. Spectral Density Functions Associated with the Tension-Dominated Spectrum Loading Imposed on Task 3 Elements.

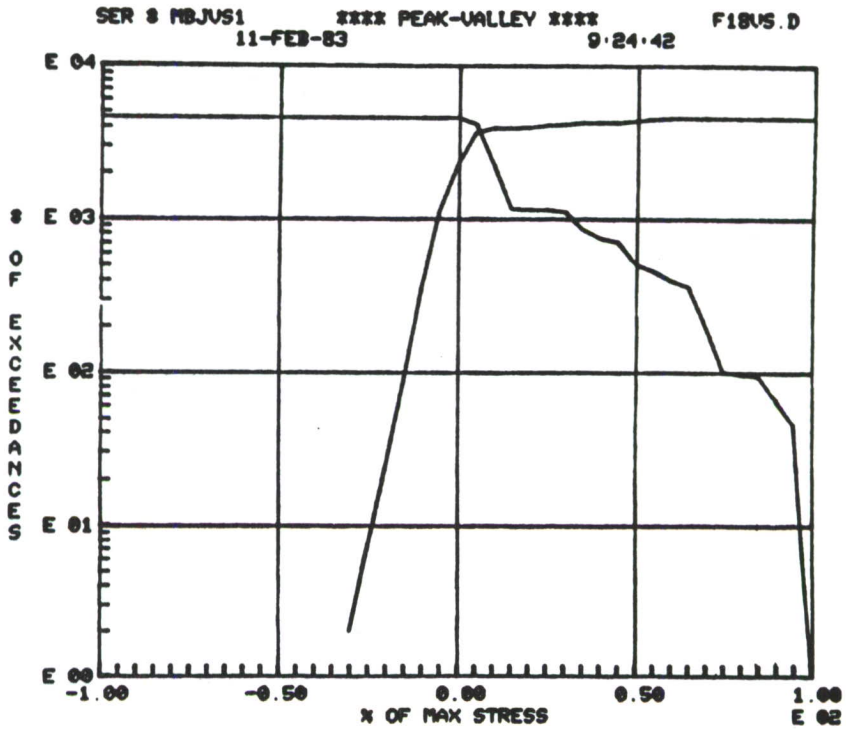

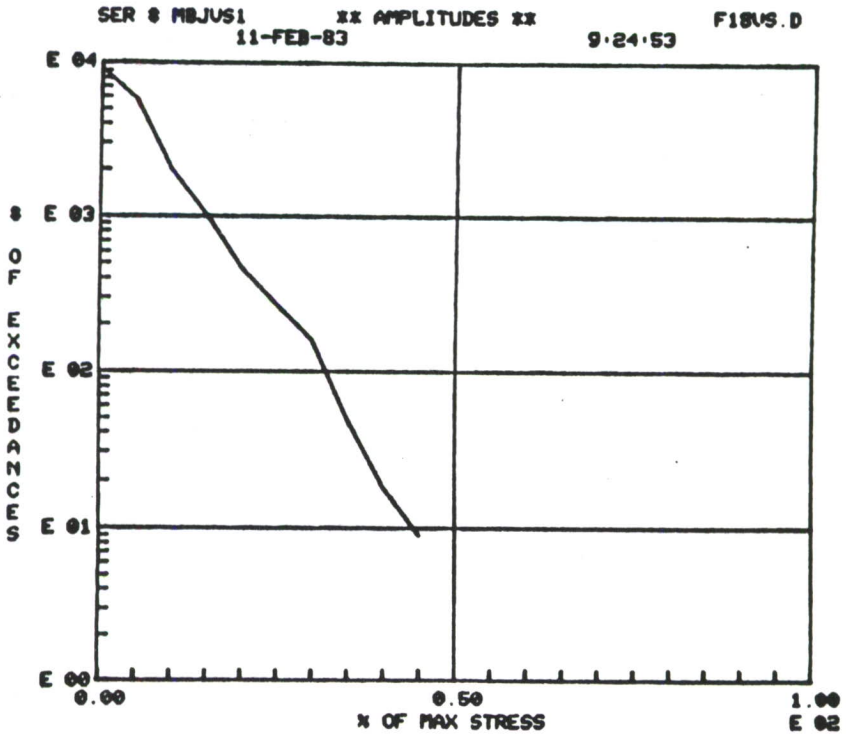

Figure 18. Exceedance Counts on Peaks, Valleys and Amplitudes in the Imposed Spectrum Loading.

Subsequently, the elements were statically tested to measure their residual tensile strengths. Strain gage readings were recorded during these tests (see Figures 13 and 14). Failure was indicated by an unloading phenomenon, accompanied by audible cracking or delaminating noise. Failed elements were photographed and examined to record failure modes. The residual static tension tests were also conducted under room temperature, dry (ambient) conditions.

3.2 Task 3 Element Test Results

Element 1 survived two lifetimes of the imposed tension-dominated spectrum load without any indication of local or gross failure. Figure 19 presents hysteresis curves obtained on the element prior to load introduction, after completing the first lifetime, and after completing the second lifetime. Hysteresis curves were obtained using data generated by the clip gage that measured the displacement between the two rows of fasteners in the graphite/epoxy tabs and the steel attachment fixture (See Figure 15). Figure 19 indicates no change in the hysteresis curves after two lifetimes of spectrum loading. The imposed spectrum load, therefore, had no deleterious effect on the element.

The element was subsequently tested to failure under static tension. The element failed at the graphite/epoxy tab location in a combined failure mode. This included severe delaminations around the fastener holes, partial shear-out, and local bearing. At 89.9 kips, a major drop in the load was recorded, indicating element failure. The load was released and the failed element was examined. Considerable tilting and "digging in" of the countersunk fasteners were noticed at every fastener location, but delaminations and other failures were not visible (See Figure 20). The element was reloaded to record the progression of failures. Many delaminations accompanied

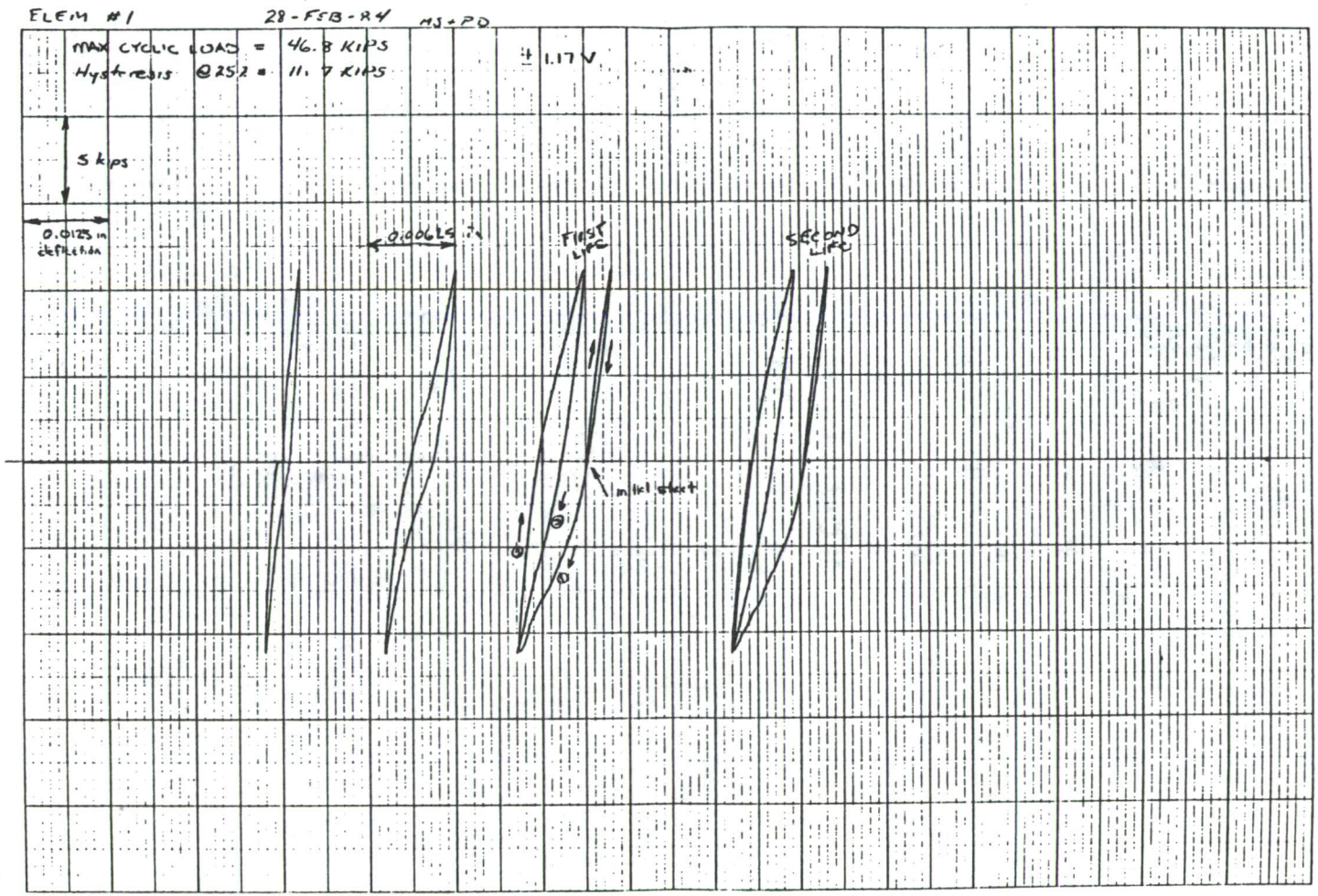

Figure 19. Hysteresis Curves for Element 1 After 0, 1 and 2 Lifetimes of Spectrum Loading.

FAILURE AT P = 89.9 KIPS

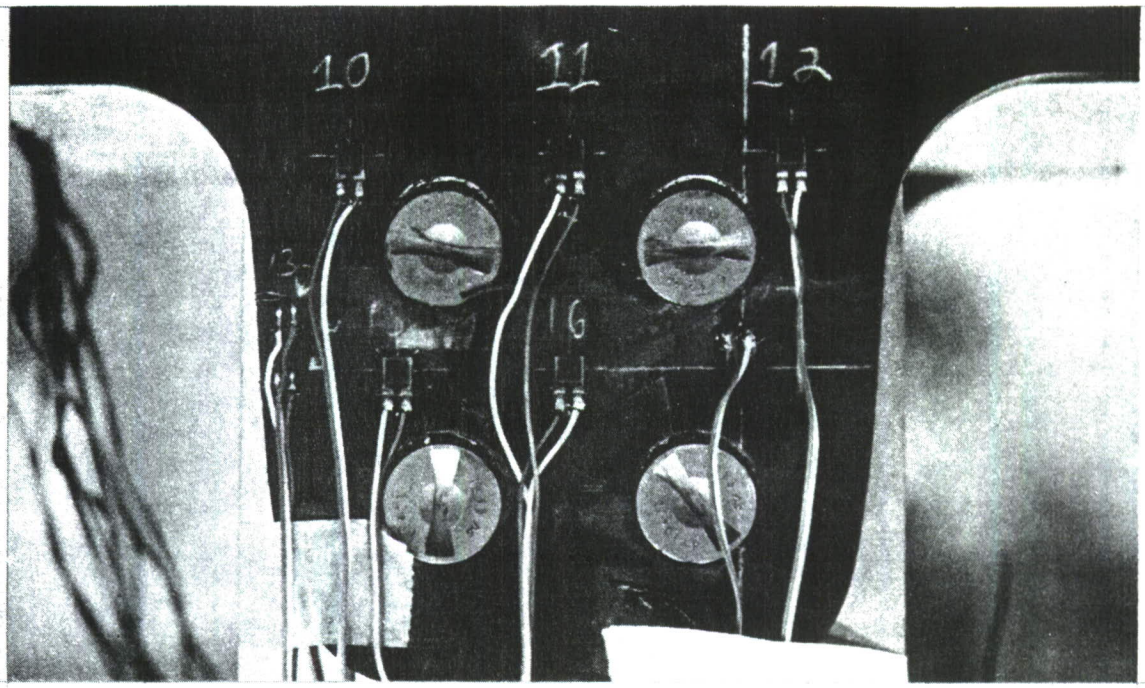

FAILURE PROGRESSION BELOW 89.9 KIPS ON RELOADING

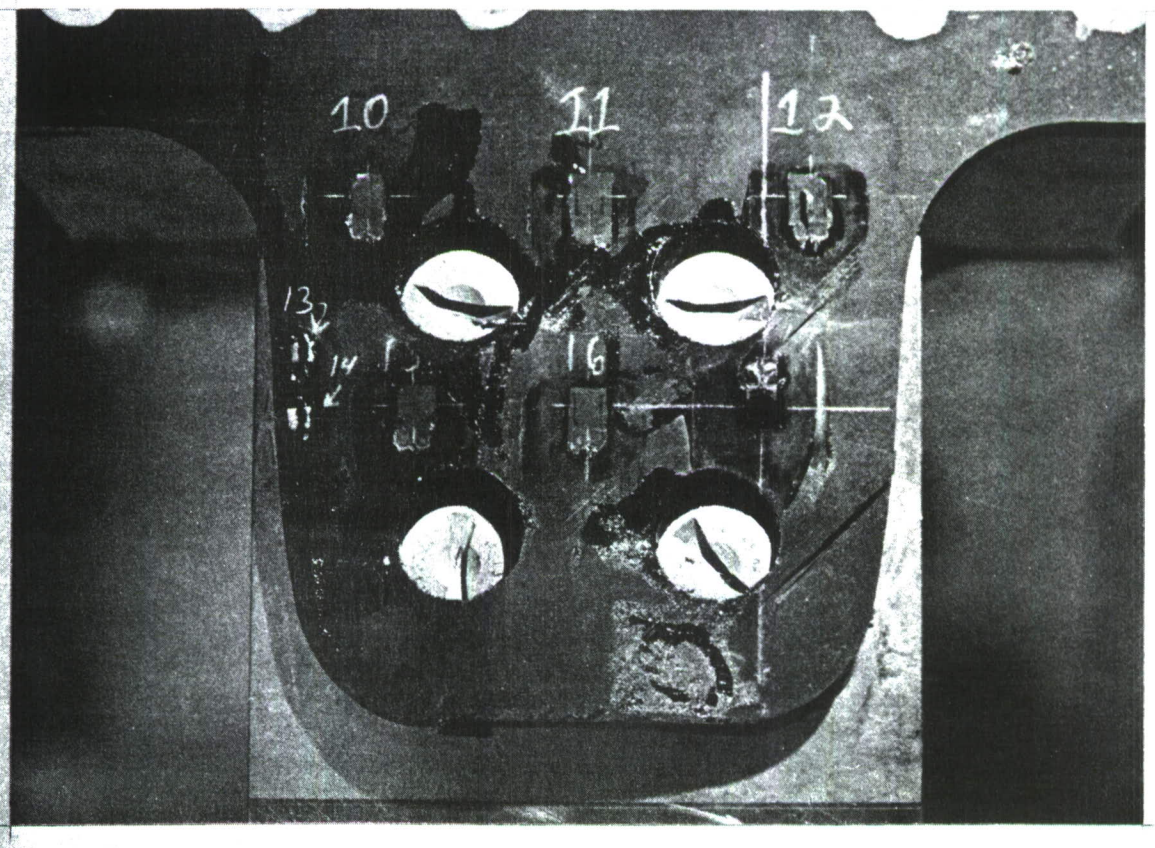

Figure 20. Failed Tab 2 in Element 1.

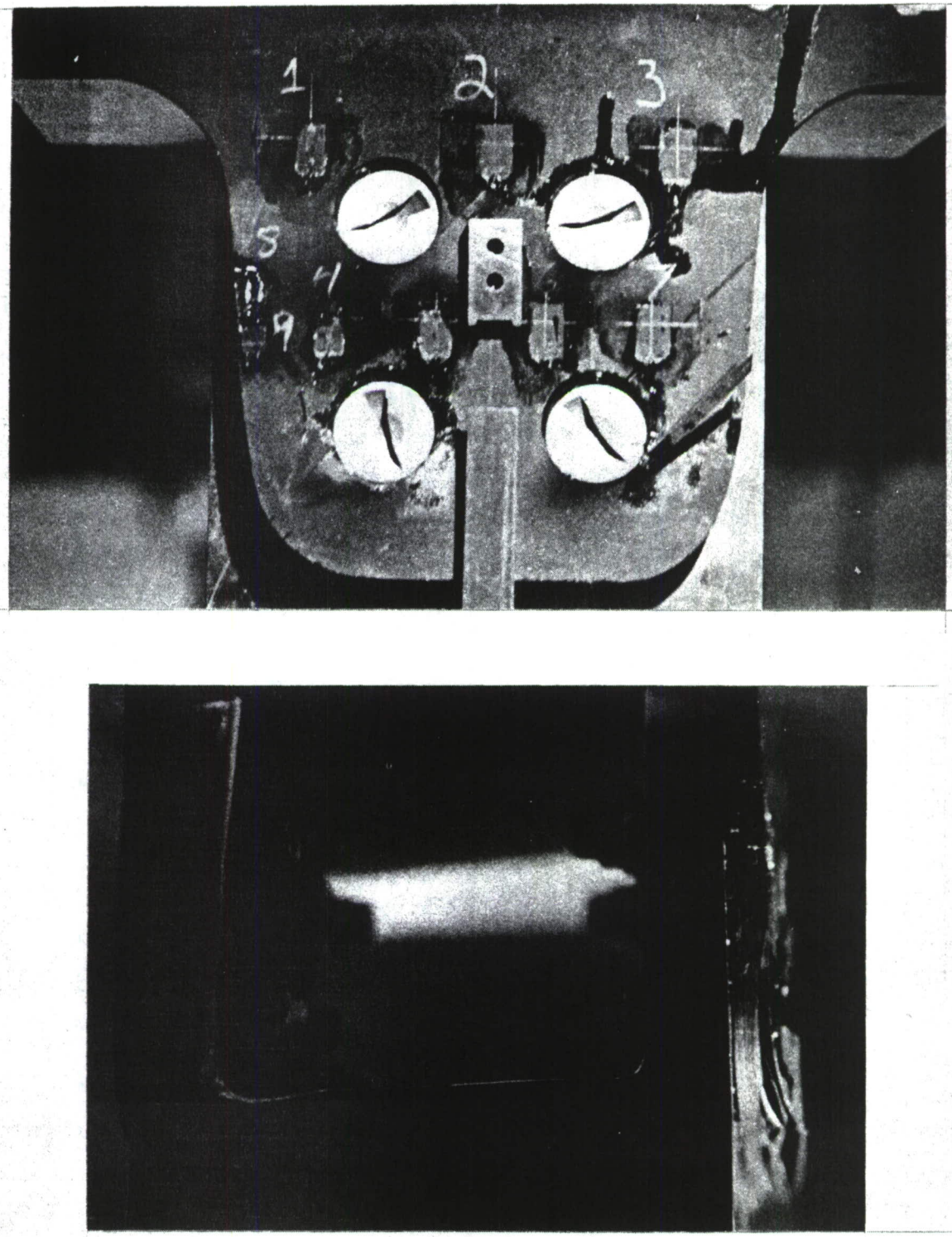

Figure 21. Failed Tab 1 in Element 1 After Reloading.

considerable digging in of the countersunk fasteners into the graphite/epoxy tabs (See Figures 20 and 21). This occurred slightly below the failure load value. The failure load (89.9 kips) for element 1 was 28% larger than the design ultimate load (70.2 kips).

Strain gage and clip gage readings obtained from element 1 during the residual tension strength test are presented in Figure 22. The tab locations these readings correspond to are presented in Figure 13. Plots of these readings as functions of the imposed load are presented in Figure 23. A summary of the readings at failure (89.9 kips) is presented in Figure 24.

Element 2 also survived two lifetimes of the imposed tension-dominated spectrum load without any indication of failure. The hysteresis curves in Figure 25 indicate that no significant damage was precipitated in the element during fatigue.

The residual static tension test on element 2 yielded a failure load of 91.8 kips. This is 31% larger than the design ultimate load of 70.2 kips. Failure occurred in the graphite/epoxy tab region of the element, in a combined mode. Photographs of the failed element tabs are presented in Figures 26 and 27. The observed failure modes are identical to those observed in element 1.

Strain gage and clip gage readings obtained from element 2 during the residual tension strength test are presented in Figure 28. The gage locations on element 2 are presented in Figure 14. Plots of readings as functions of the imposed load are presented in Figure 29. A summary of the readings at failure (91.8 kips) is presented in Figure 30.

In summary, both the elements failed above the design ultimate load (70.2 kips), with a 28 to 31% margin of safety. The analytical procedure used in the preliminary design of these elements is, therefore, adequate to establish the applicability of this design at the subcomponent level.

*** TABULARIZED RESULTS FOR SPECIMEN @ELEM @1 : ***

LOAD	@6	@7	@1	@2	@3	@4	@5
3.6	84	74	27	45	9	93	84
7.2	148	138	72	21	26	167	157
10.8	225	208	124	79	58	256	239
14.4	309	272	178	116	112	311	328
18.0	394	328	244	140	178	376	413
21.6	479	384	318	251	253	452	497
25.2	552	436	389	300	324	522	549
28.8	626	494	466	376	408	600	615
32.39	684	542	551	446	486	667	675
36.0	755	592	639	527	572	728	743
39.59	816	641	726	593	656	795	812
43.2	888	683	821	689	740	853	879
46.8	958	740	909	757	825	922	929
50.4	1015	782	999	870	910	993	1000
54.0	1085	824	1092	950	1003	1068	1061
57.6	1148	867	1190	1047	1093	1135	1120
61.19	1212	928	1286	1208	1209	1187	1174
64.79	1277	996	1391	1328	1301	1246	1230
68.4	1322	1056	1489	1462	1393	1270	1241
72.0	1352	1124	1603	1580	1500	1289	1220
75.6	1446	1236	1722	1707	1625	1503	1340
79.19	1442	1161	1849	1835	1727	1615	1414
82.8	1791	1338	1995	1954	1845	1795	1670
86.4	1965	1436	2115	2138	1978	1979	1790
89.88	1972	1489	2334	2367	2100	1346	1446

LOAD	15	16	17	CLIP GAGE	@8	@9
3.6	73	89	80	-2328	143	88
7.2	161	198	161	-1880	241	154
10.8	239	295	206	-1309	369	240
14.4	290	411	244	-563	502	337
18.0	338	546	272	334	646	429
21.6	387	693	300	1353	773	522
25.2	441	835	319	2372	905	613
28.8	470	960	349	3620	1042	692
32.39	512	1084	375	4966	1188	770
36.0	545	1199	413	6190	1335	854
39.59	595	1317	444	7427	1482	942
43.2	639	1436	488	8651	1622	1017
46.8	677	1537	530	9851	1757	1096
50.4	724	1647	561	11160	1891	1184
54.0	780	1767	610	12699	2033	1256
57.6	839	1914	670	14626	2173	1321
61.19	904	2087	742	16995	2295	1365
64.79	948	2255	789	19470	2441	1458
68.4	956	2433	756	22366	2583	1512
72.0	947	2592	704	26007	2690	1560
75.6	876	2909	708	31473	2794	1707
79.19	818	3174	704	36892	2925	1835
82.8	743	3467	911	43795	3068	1941
86.4	502	3764	722	52286	3176	2079
89.88	-433	4252	-292	71419	3393	2127

LOAD	@13	@14	@10	@11	@12
3.6	124	115	74	50	88
7.2	229	198	131	68	156
10.8	350	277	205	119	233
14.4	477	359	304	207	322
18.0	617	457	387	292	399
21.6	754	553	476	377	479
25.2	896	660	566	474	575
28.8	1041	744	668	576	668
32.39	1178	844	769	668	778
36.0	1324	941	870	776	870
39.59	1464	1042	972	884	979
43.2	1617	1134	1077	989	1076
46.8	1755	1235	1175	1096	1174
50.4	1904	1323	1288	1202	1277
54.0	2050	1426	1403	1342	1386
57.6	2206	1528	1519	1484	1499
61.19	2340	1599	1653	1668	1624
64.79	2483	1694	1774	1814	1744
68.4	2619	1781	1906	1983	1875
72.0	2758	1879	2037	2145	1979
75.6	2928	2042	2208	2357	2138
79.19	3024	2226	2394	2532	2308
82.8	3195	2411	2577	2716	2490
86.4	3287	2525	2706	2926	2637
89.88	3325	2527	2887	3213	2744

Figure 22. Strain Gage and Clip Gage Readings from Element 1 (See Figure 13).

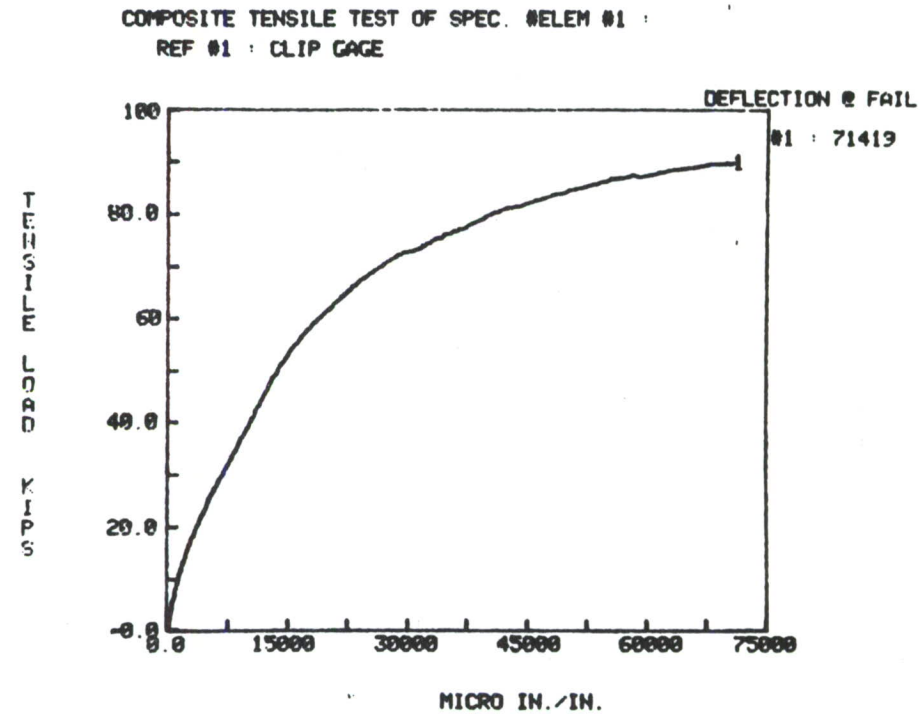

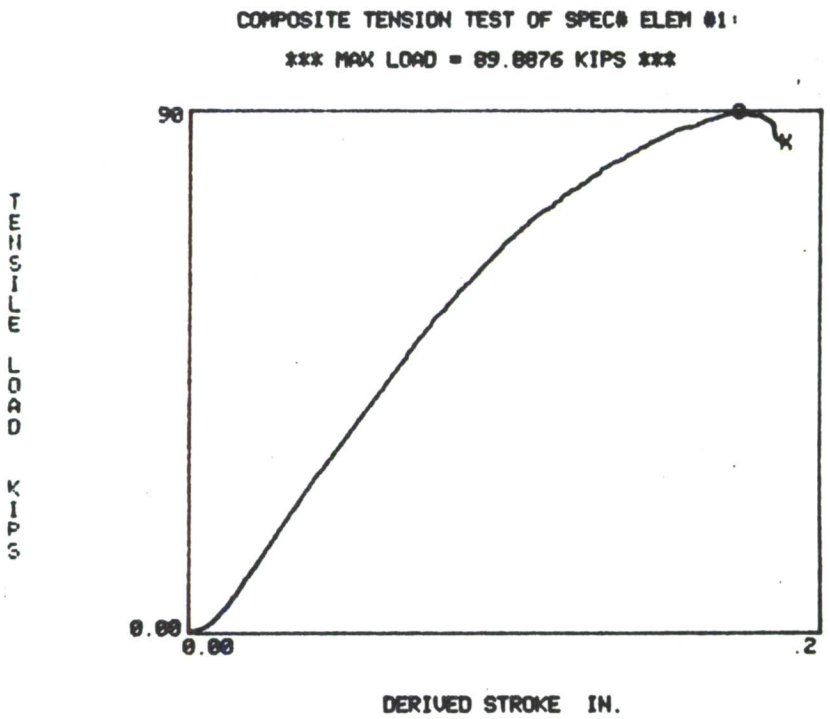

Figure 23. Strain Variations with Imposed Load for Element 1.

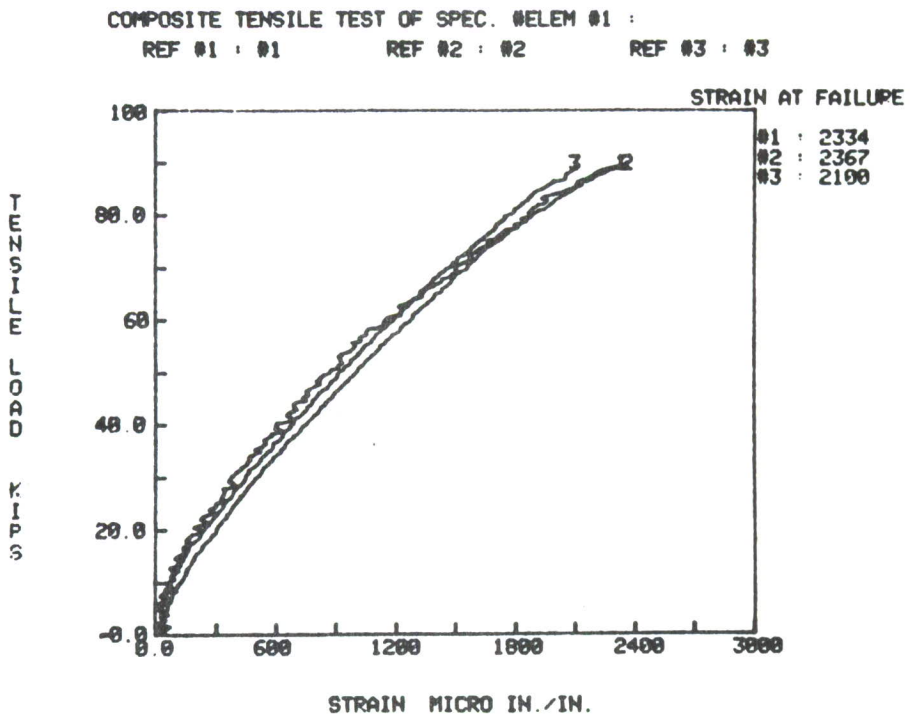

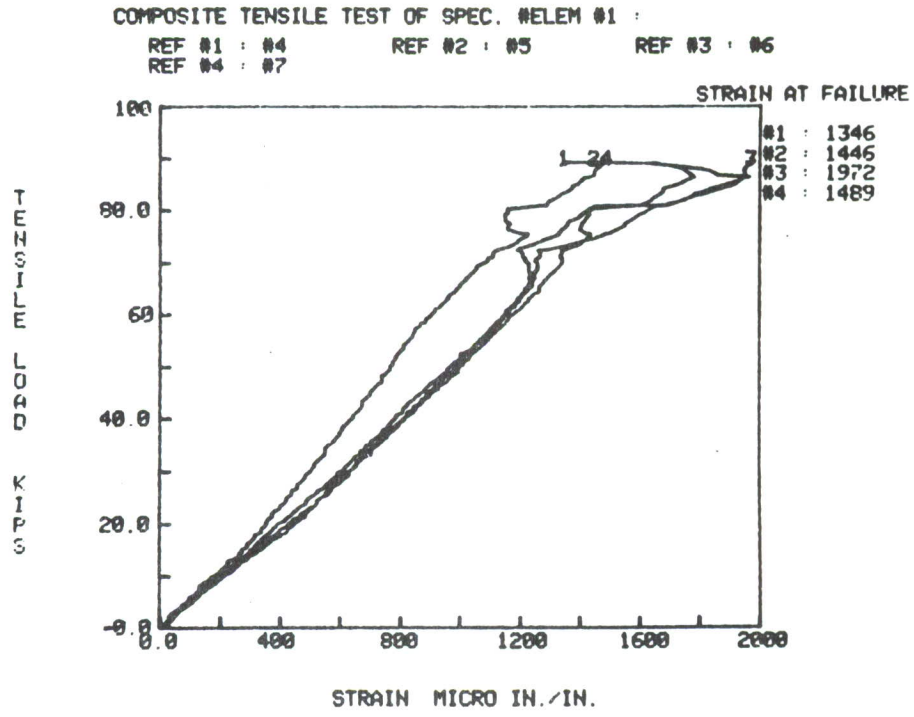

Figure 23. Strain Variations with Imposed Load for Element 1 (Continued).

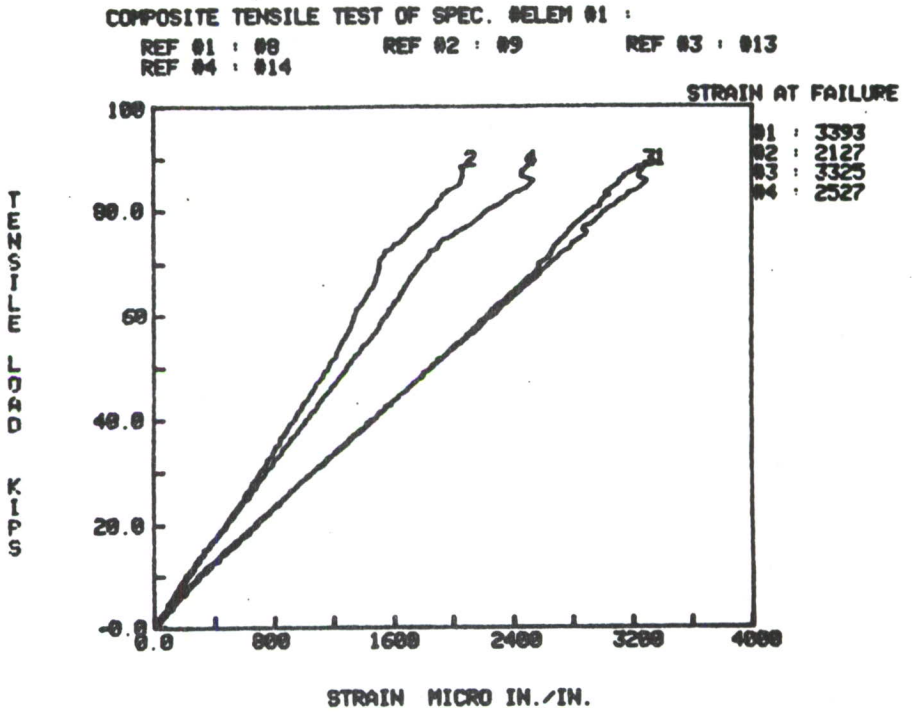

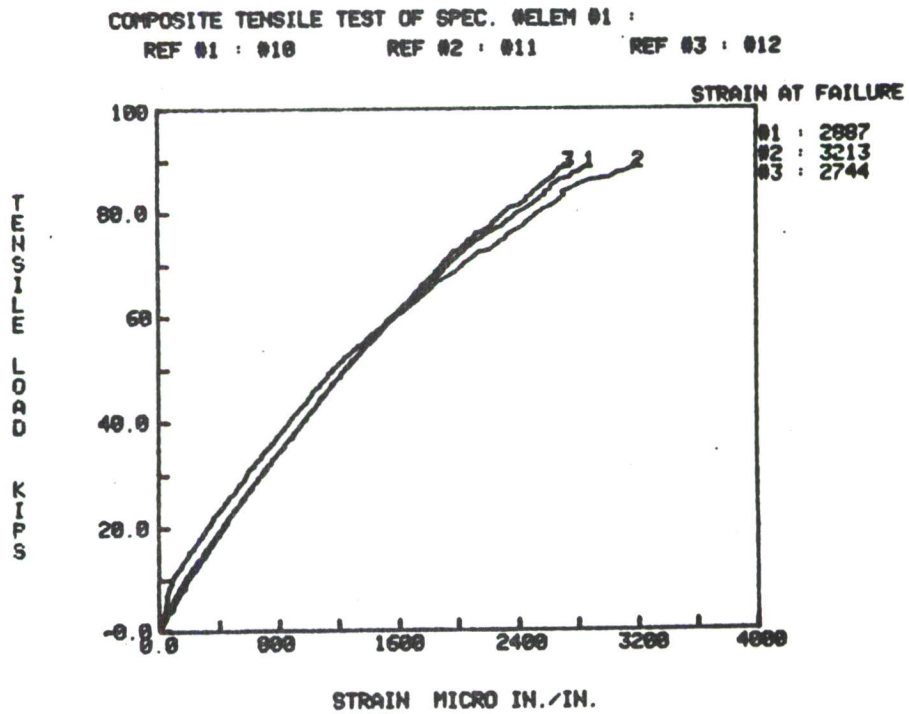

Figure 23. Strain Variations with Imposed Load for Element 1 (Continued).

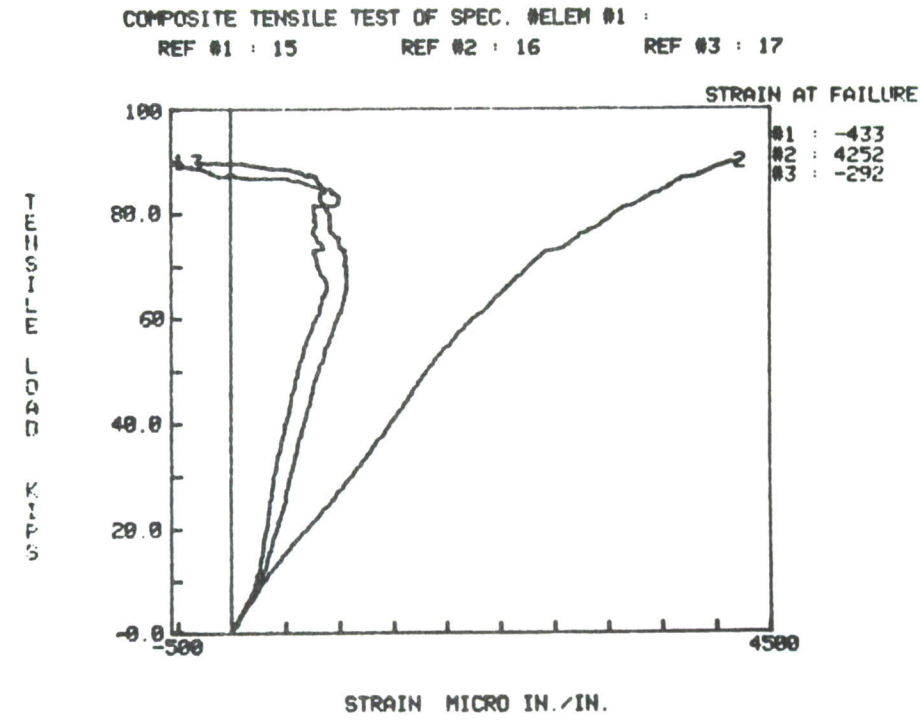

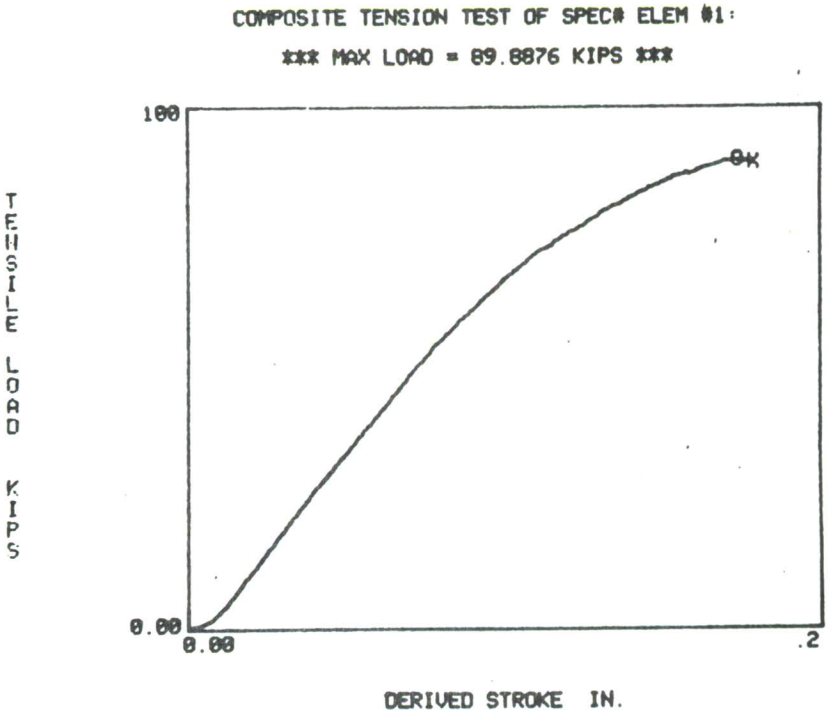

Figure 23. Strain Variations with Imposed Load for Element 1. (Concluded).

TEST DATE
2-MAR-84

REQUESTOR COPY

*** COMPOSITE TENSILE TEST RESULTS ***
DATA FILE:D00213

SPEC ID: ELEM #1 MATERIAL :

WIDTH : 1 IN. THICKNESS : 1 IN.

TEST TEMP.(F) : RT ENVIRONMENT : LA

ULTIMATE LOAD = 89.8876 KIPS

GAGE ID	STRAIN AT FAILURE
#4	1346.14
#5	1446.41
#6	1972.38
#7	1489.43
#1	2334.86
#2	2367.21
#3	2100.68

TEST DATE
2-MAR-84

REQUESTOR COPY

*** COMPOSITE TENSILE TEST RESULTS ***
DATA FILE:D00213

SPEC ID: ELEM #1 MATERIAL :

WIDTH : 1 IN. THICKNESS : 1 IN.

TEST TEMP.(F) : RT ENVIRONMENT : LA

ULTIMATE LOAD = 89.8876 KIPS

GAGE ID	STRAIN AT FAILURE
15	-432.653
16	4252.15
17	-291.332
CLIP GAGE	71420
#8	3393.88
#9	2127.57
#13	3325.94
#14	2527.46
#10	2887.71
#11	3213.83
#12	2744.58

Figure 24. Summary of Strains at Failure for Element 1.

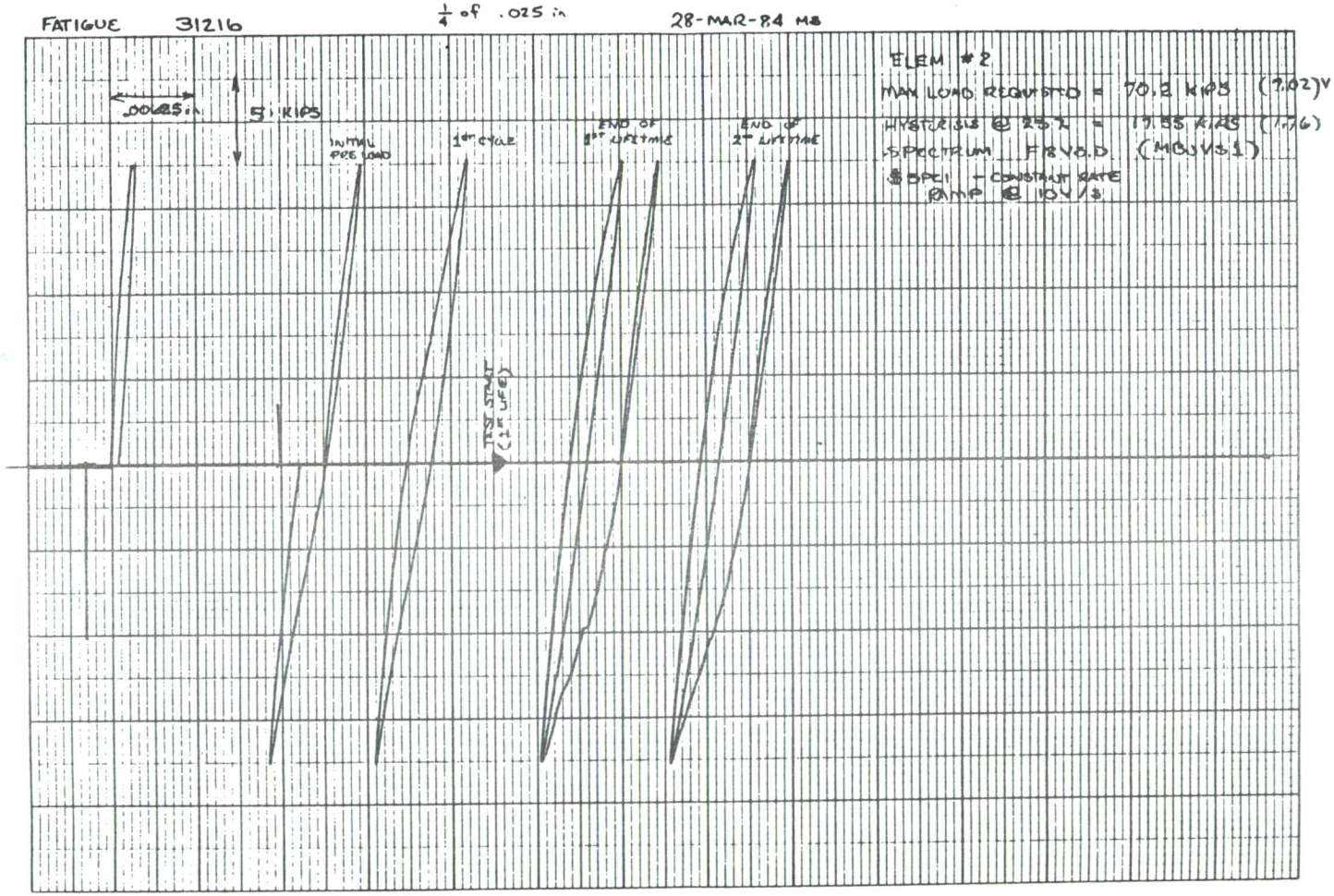

Figure 25. Hysteresis Curves for Element 2 After 0, 1 and 2 Lifetimes of Spectrum Loading.

TAB 1

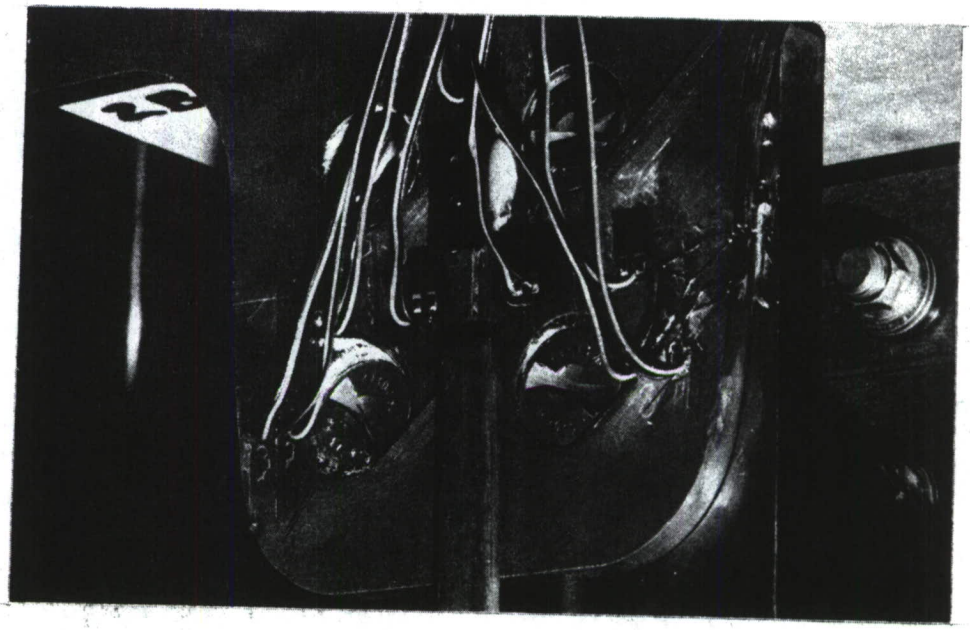

TAB 2

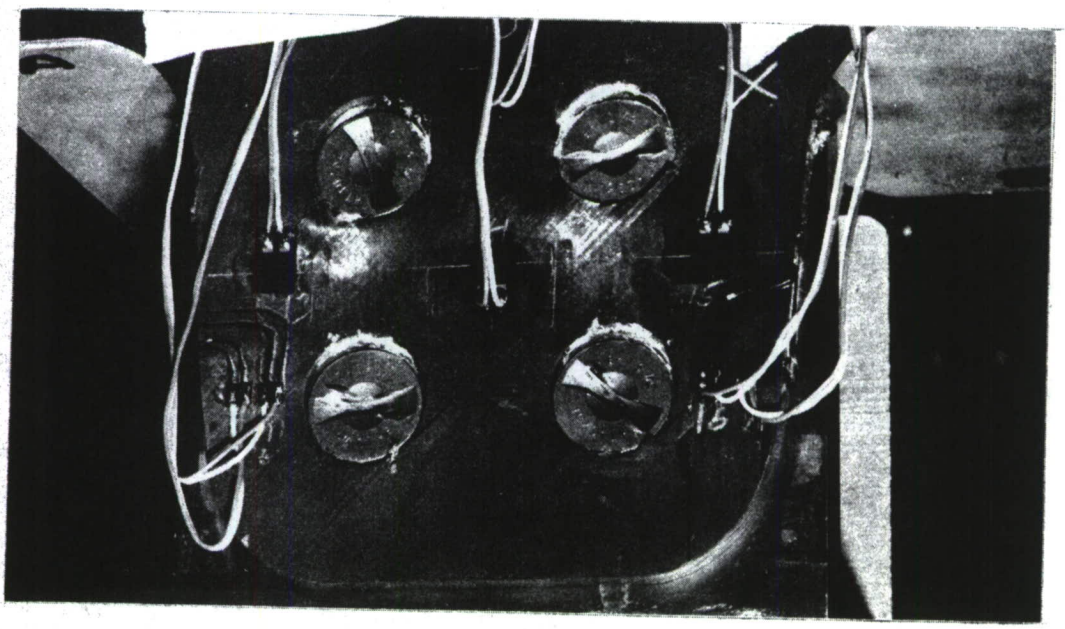

Figure 26. Failed Element 2 Tabs.

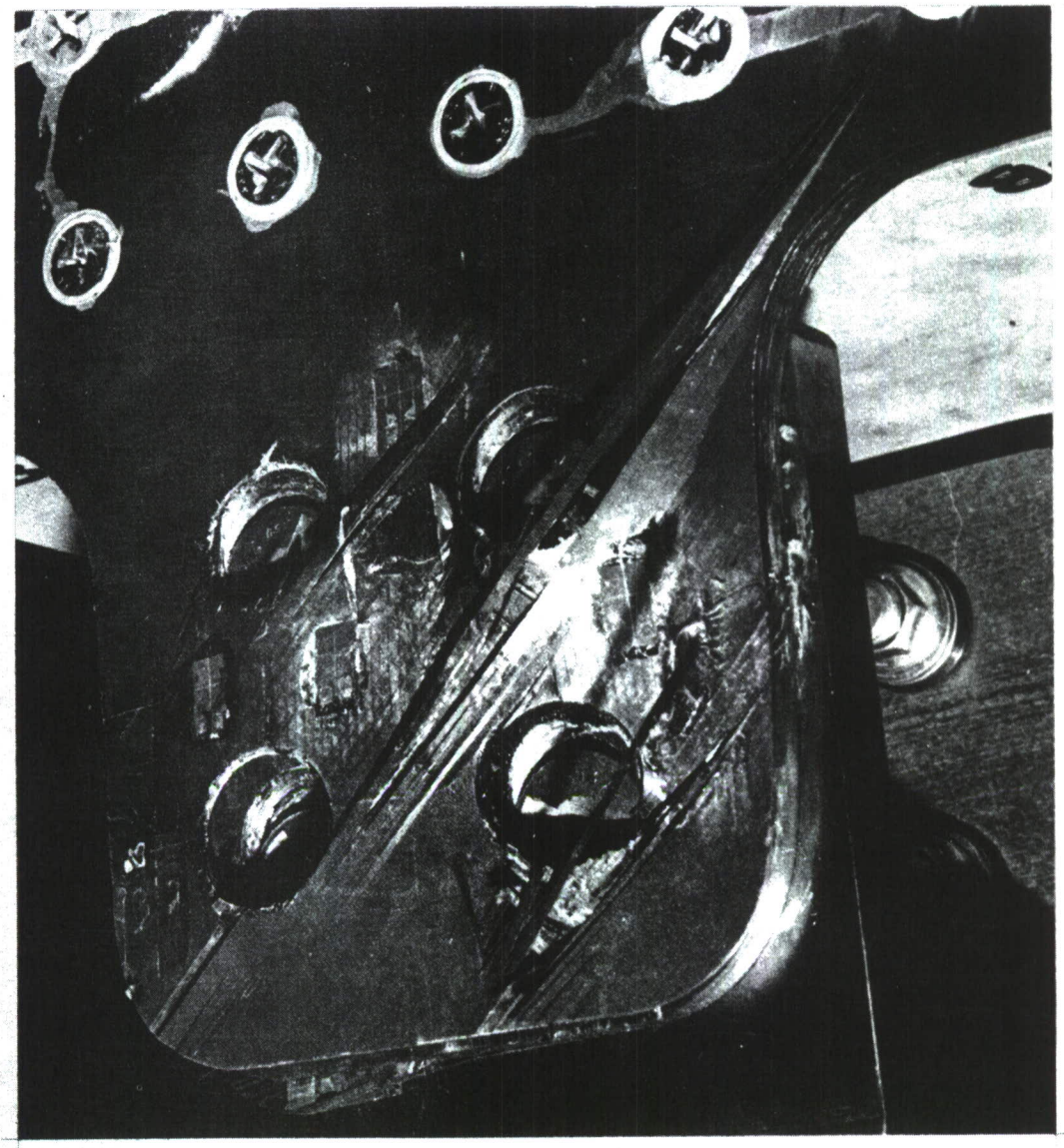

Figure 27. Progression of Element 2 Failure During Reloading.

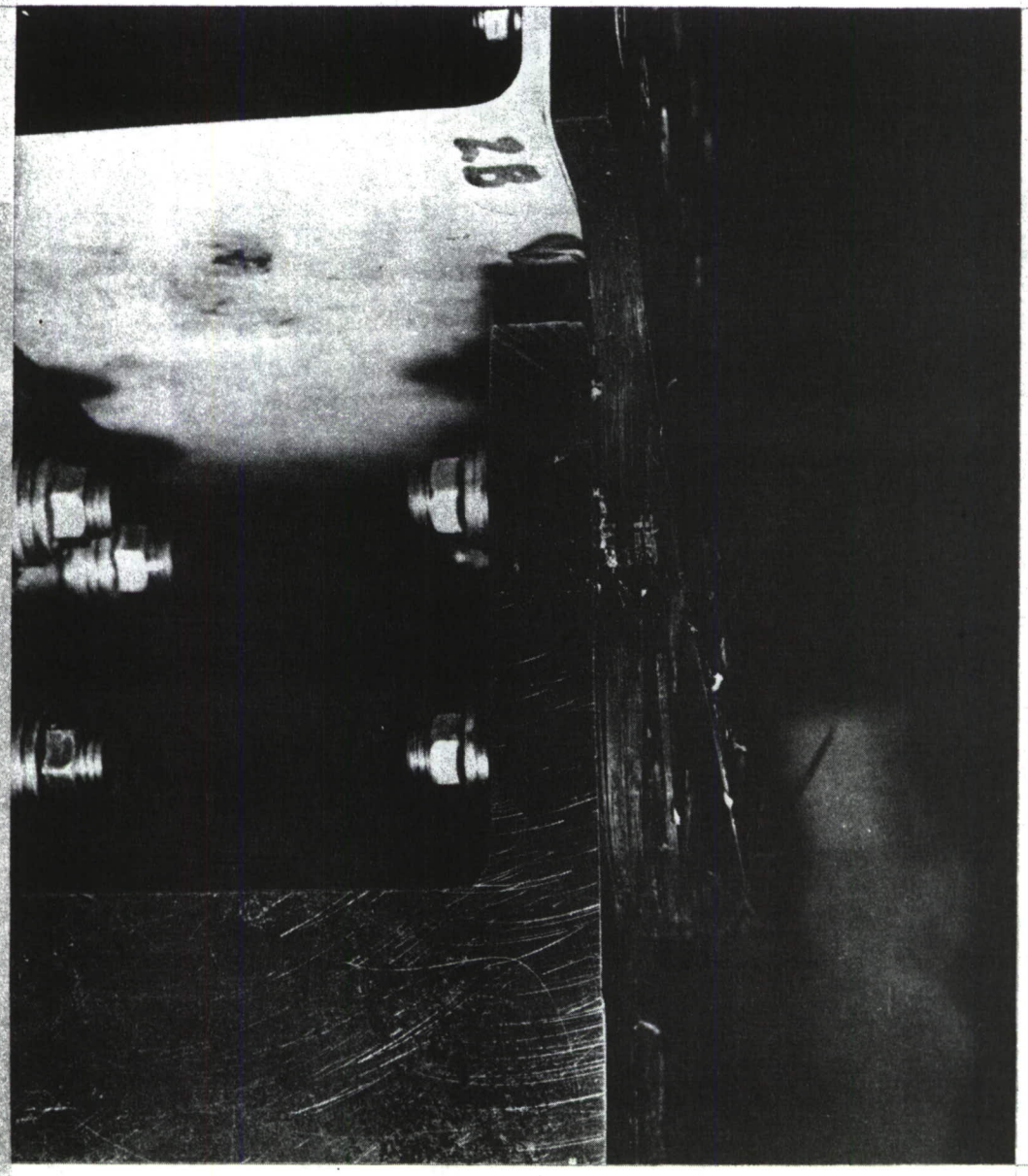

Figure 27. Progression of Element 2 Failure During Reloading (Concluded).

••• TABULARIZED RESULTS FOR SPECIMEN 0ELEM. 02 ! •••

LOAD	06	07	010	012	017	04	05
3.68	121	101	56	83	120	112	112
7.36	202	183	87	183	234	190	202
11.04	291	262	141	301	353	254	300
14.72	374	364	215	413	491	319	395
18.4	459	454	309	535	645	352	516
22.08	533	534	421	667	795	383	628
25.76	582	606	552	785	973	376	731
29.44	631	675	682	908	1159	413	820
33.12	670	731	816	1051	1332	423	912
36.8	721	796	948	1212	1504	433	1005
40.48	752	853	1083	1355	1656	452	1092
44.16	803	928	1224	1497	1819	479	1186
47.84	847	995	1366	1648	1973	490	1270
51.52	898	1072	1498	1796	2131	511	1360
55.2	939	1137	1636	1937	2286	523	1445
58.88	986	1216	1770	2073	2442	533	1530
62.56	1030	1292	1906	2208	2598	536	1616
66.24	1068	1369	2039	2357	2756	553	1698
69.92	1119	1445	2193	2484	2912	564	1788
73.6	1164	1533	2370	2639	3068	579	1867
77.28	1211	1612	2525	2765	3206	583	1951
80.96	1258	1698	2732	2898	3347	600	2042
84.64	1279	1746	2913	3025	3463	618	2133
88.32	1230	1931	3254	3075	3476	677	2407
91.84	1258	2081	3414	2944	3532	545	2896

LOAD	13	14	15	CLIP GAGE	02	08
3.68	65	68	87	322	130	89
7.36	139	158	176	829	218	165
11.04	214	257	266	1413	297	241
14.72	299	365	346	2049	370	333
18.4	384	493	449	2867	446	405
22.08	469	638	562	3805	545	495
25.76	532	811	693	5274	613	594
29.44	584	954	780	7131	700	675
33.12	636	1086	858	8722	780	752
36.8	694	1209	931	10208	869	855
40.48	740	1331	1001	11625	945	927
44.16	788	1445	1072	12975	1030	1018
47.84	844	1568	1152	14303	1115	1115
51.52	892	1677	1223	15580	1191	1190
55.2	929	1785	1293	16792	1273	1282
58.88	990	1898	1373	18097	1352	1360
62.56	1042	2002	1453	19338	1431	1442
66.24	1089	2106	1524	20586	1506	1542
69.92	1137	2211	1604	21890	1588	1629
73.6	1189	2324	1684	23255	1670	1707
77.28	1239	2463	1753	24934	1747	1771
80.96	1318	2616	1831	27004	1840	1849
84.64	1401	2781	1918	30036	1965	1888
88.32	1844	3509	2385	41886	2174	2052
91.84	2384	4097	2784	65241	2268	2211

LOAD	011	016	01	03	09
3.68	70	94	56	104	128
7.36	138	175	93	203	231
11.04	223	259	150	325	381
14.72	287	342	224	471	510
18.4	359	429	322	606	639
22.08	436	525	419	761	788
25.76	473	629	543	907	928
29.44	523	717	679	1065	1092
33.12	576	797	807	1235	1256
36.8	630	879	936	1420	1440
40.48	667	953	1066	1592	1608
44.16	728	1024	1196	1755	1774
47.84	785	1104	1324	1928	1918
51.52	827	1170	1465	2100	2069
55.2	882	1261	1586	2266	2224
58.88	936	1342	1722	2419	2371
62.56	976	1421	1851	2611	2532
66.24	1022	1502	1990	2749	2662
69.92	1068	1584	2123	2916	2815
73.6	1132	1668	2260	3080	2948
77.28	1177	1722	2403	3248	3090
80.96	1198	1788	2571	3396	3220
84.64	1262	1844	2768	3565	3346
88.32	1412	1966	2994	3687	3360
91.84	1589	2013	3088	3548	3426

Figure 28. Strain Gage and Clip Gage Readings from Element 2 (See Figure 14).

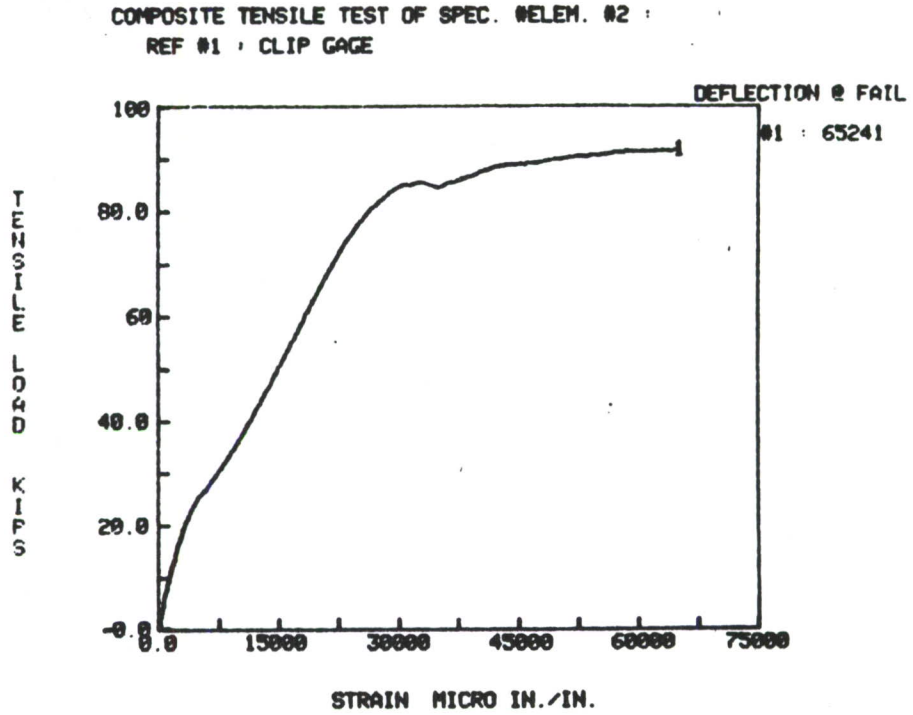

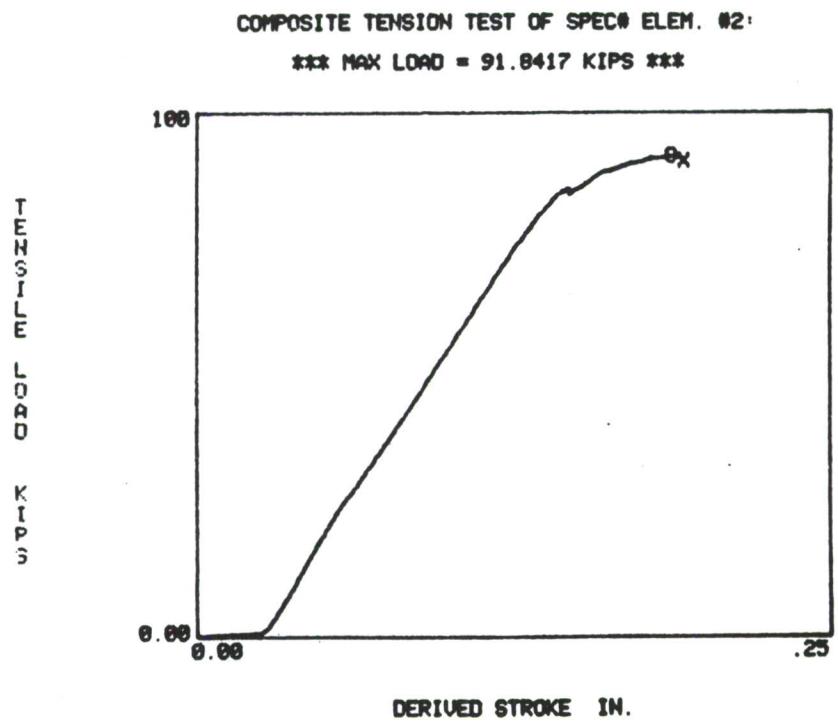

Figure 29. Strain Variations with Imposed Load for Element 2.

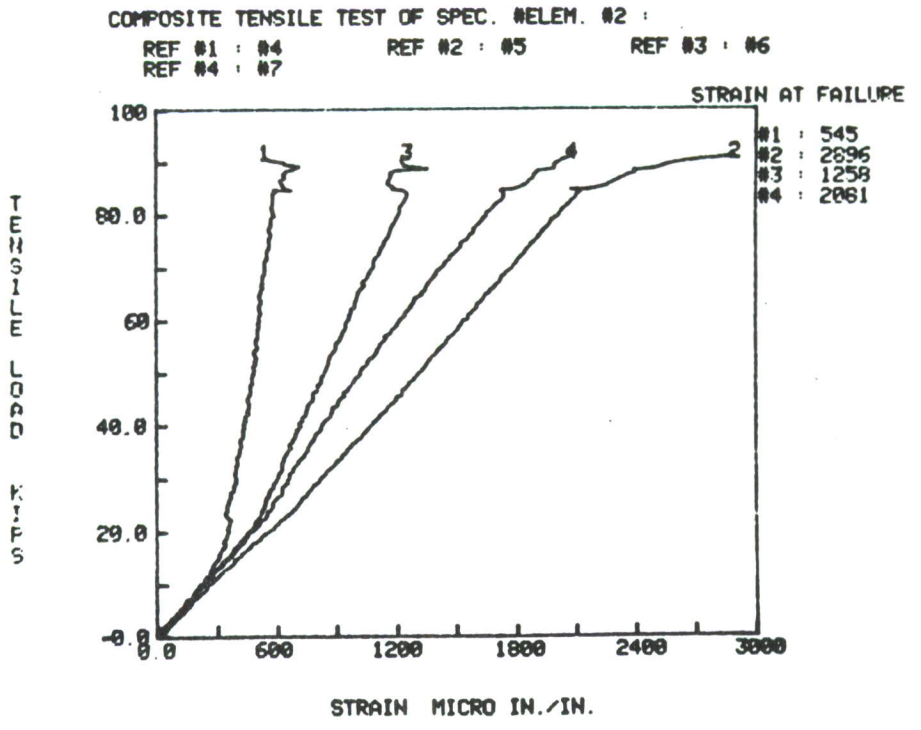

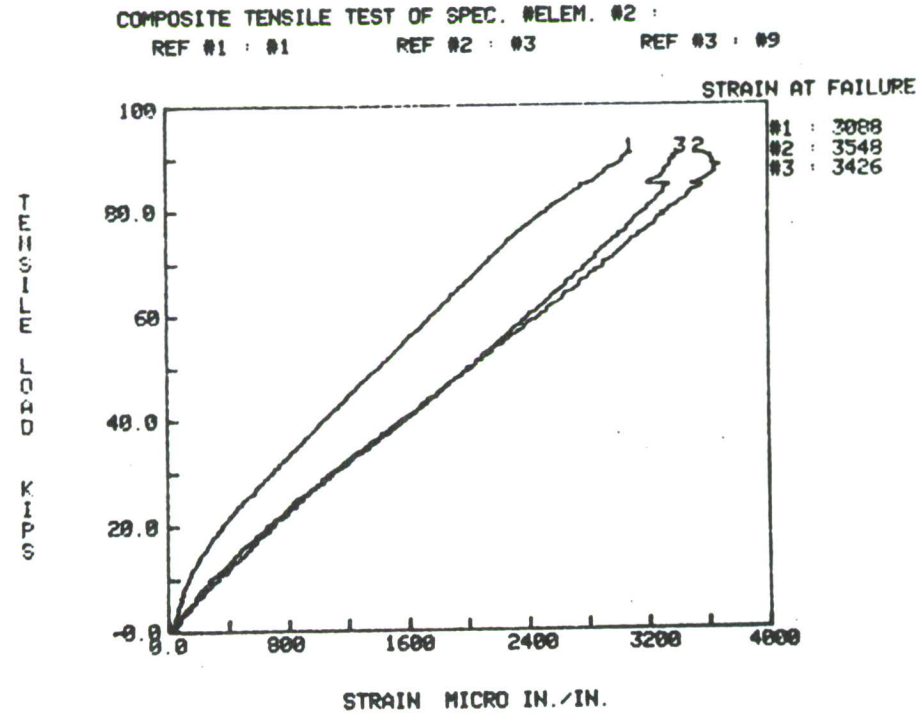

Figure 29. Strain Variations with Imposed Load for Element 2 (Continued).

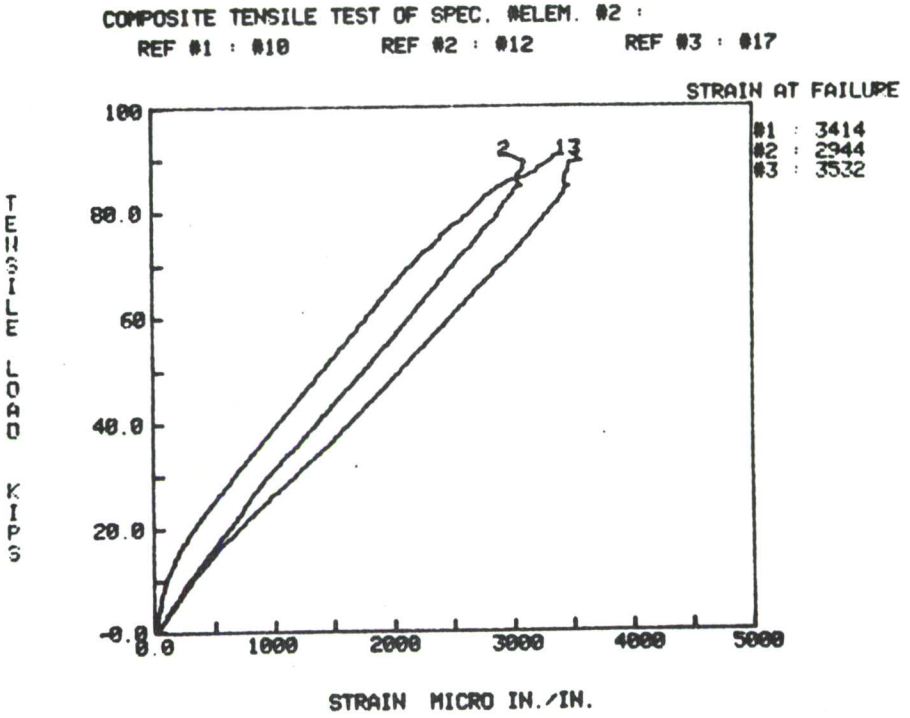

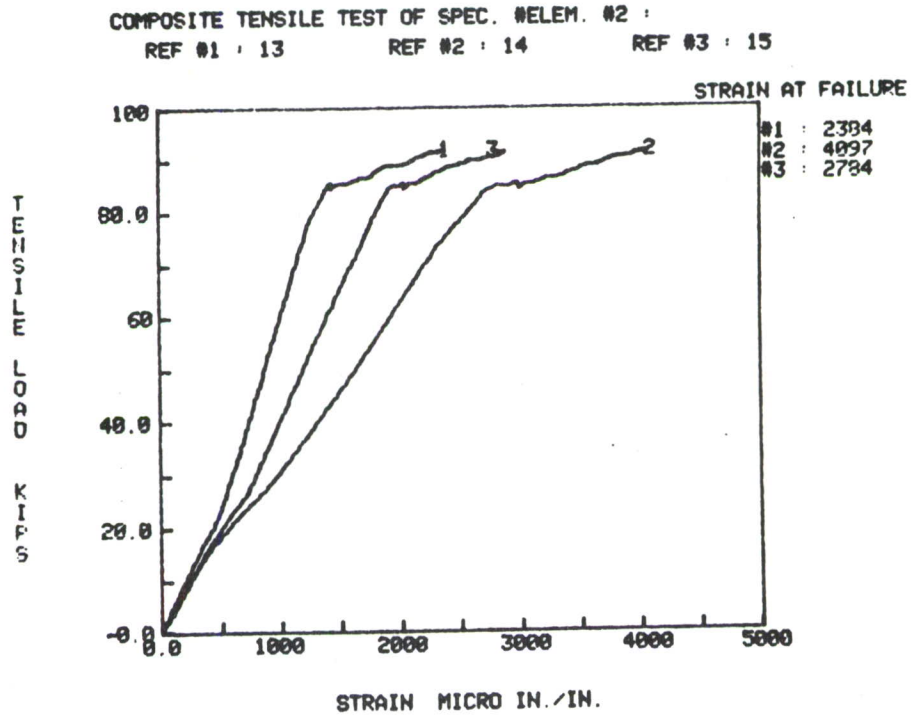

Figure 29. Strain Variations with Imposed Load for Element 2 (Continued).

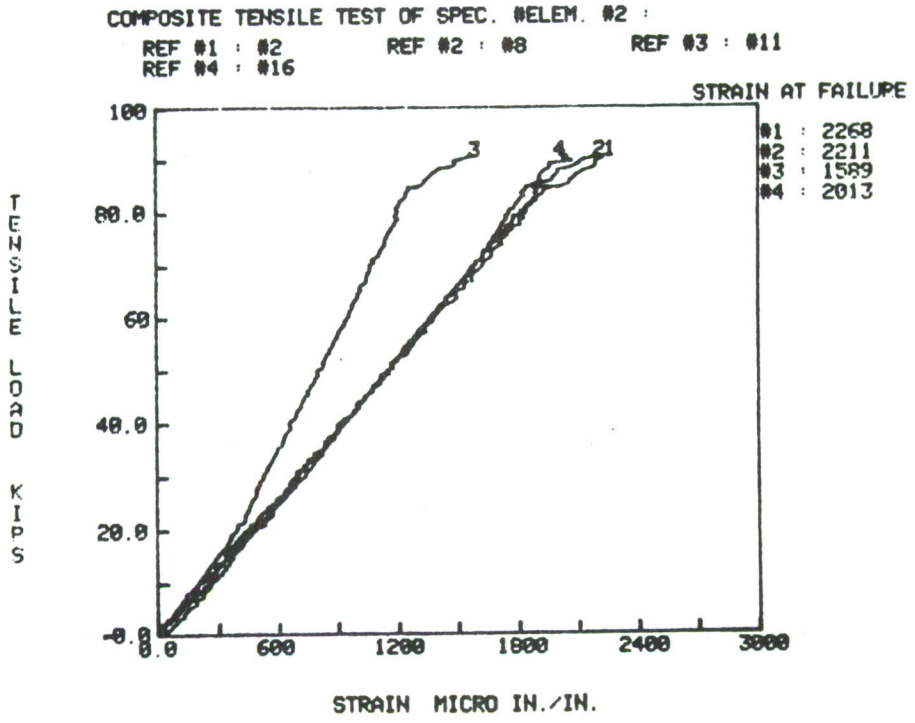

Figure 29. Strain Variations with Imposed Load for Element 2 (Concluded).

TEST DATE 29-MAR-84 REQUESTOR COPY

*** COMPOSITE TENSILE TEST RESULTS ***
DATA FILE:D00227

SPEC ID: ELEM. #2 MATERIAL :

WIDTH : 1 IN. THICKNESS : 1 IN.

TEST TEMP.(F) : RT ENVIRONMENT : LA

ULTIMATE LOAD = 91.8417 KIPS

GAGE ID	STRAIN AT FAILURE
13	2384.95
14	4097.28
15	2784.41
CLIP GAGE	65241.4
#2	2268.43
#8	2211.53
#11	1589.27
#16	2013.26
#1	3088.86
#3	3548.63
#9	3426.04

TEST DATE 29-MAR-84 REQUESTOR COPY

*** COMPOSITE TENSILE TEST RESULTS ***
DATA FILE:D00227

SPEC ID: ELEM. #2 MATERIAL :

WIDTH : 1 IN. THICKNESS : 1 IN.

TEST TEMP.(F) : RT ENVIRONMENT : LA

ULTIMATE LOAD = 91.8417 KIPS

GAGE ID	STRAIN AT FAILURE
#4	545.71
#5	2896.78
#6	1258.42
#7	2081.69
#10	3414.73
#12	2944.37
#17	3532.25

Figure 30. Summary of Strains at Failure for Element 2.

SECTION 4

ANALYSIS OF TASK 3 ELEMENT

Reference 3 presents a description of the strength analysis (SAMCJ computer code) developed in this program for multifastener joints in composite structures. The Task 3 test element is analyzed below, using the SAMCJ code, to predict its tensile strength, the failure location and the failure mode. Analytical predictions are compared with the test results in Section 3. Though the analysis was performed retrospectively, the assumed material and failure parameters are identical to those used in Reference 4.

Refer to Figures 5 to 8 for details of the test element. The element, when loaded in tension (see Figure 16), failed in the skin tab region (see Figures 26 and 27). Of the two test elements, the skins of only the second element were machined uniformly to yield a symmetric loading situation (see Figures 11 and 12). The critical skin-to-fuselage joint in element 2 is, therefore, analyzed using the SAMCJ code.

Figure 31 presents the dimensions of the skin tabs in element 2 and the fuselage attachment frame. The skin has a [0 /+-45 /90] layup at the top of the tab region. Across the top row of fasteners, it has an average of 58 plies, and across the bottom row of fasteners, it has an average of 52 plies. Figure 7 includes the stacking sequence for the unmachined skin layup. For analytical purposes, the tapered tabs region is modeled as two uniform regions of different thicknesses. The top region is modeled to contain a [0 /+-45 /90] layup, and the bottom region is assumed to be a [0 /+-45 /90] laminate. The average thickness of a ply in the skin was measured to be 0.0049 inch. The fuselage attachment frame is,

Fuselage
Attachment
Frame

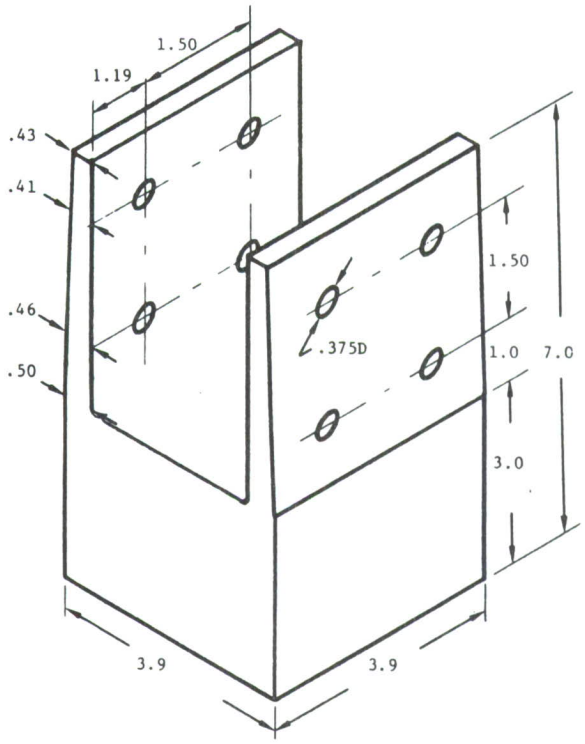

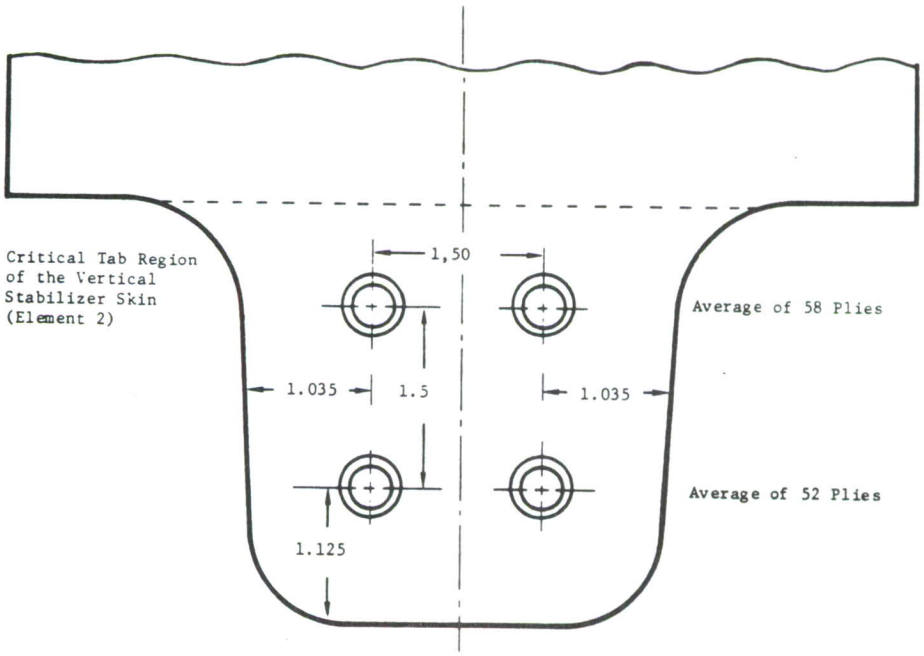

Figure 31. Dimensions of the Critical Skin Tab and the Fuselage Attachment Frame.

likewise, divided into a 0.41-inch-thick region and a 0.46-inch-thick region (see Figure 31).

The modeled joint segment is half of the symmetric skin tab-to-fuselage attachment. The total joint failure load is, therefore, twice the predicted load. A single shear load transfer between the AS4/3501-6 graphite/epoxy skin tab and the steel attachment frame is analyzed. The graphite/epoxy tab and the steel plate are divided into four elements each. The average width of the slightly tapered tab is used in the analytical model (3.57 in.). The fiber-directional tensile and compressive failure strains for AS4/3501-6 graphite/epoxy are assumed to be 0.012 and 0.0175, respectively (References 4, 9). The characteristic distances for net section, bearing and shear-out failure modes are assumed to be 0.10, 0.25 and 0.25 inch, respectively (Reference 4). The basic AS4/3501-6 lamina properties are assumed to be 18.5 Msi, 1.9 Msi and 0.85 Msi for E_{11}, E_{22} and G_{12}, respectively, and 0.3 for the major Poisson ratio.

The skins are attached to the fuselage frame by 3/8-inch-diameter, countersunk fasteners (100 degree tension head). The effect of countersunk fasteners is accounted for by assuming free rotation at the fastener head location, and by using an average fastener diameter of 0.458 inch to account for the countersunk depth in the tabs.

Analytically predicted load distribution among the fasteners in each tab is presented in Figure 32. The symmetry in the fastener arrangement results in low values for the transverse components of fastener loads (perpendicular to the load direction). Also, the loads in the top row of fasteners are approximately 14% larger than those in the botton row of fasteners. This leads to a prediction of failure initiation from the top row of fasteners (see Figure 32). The predicted load

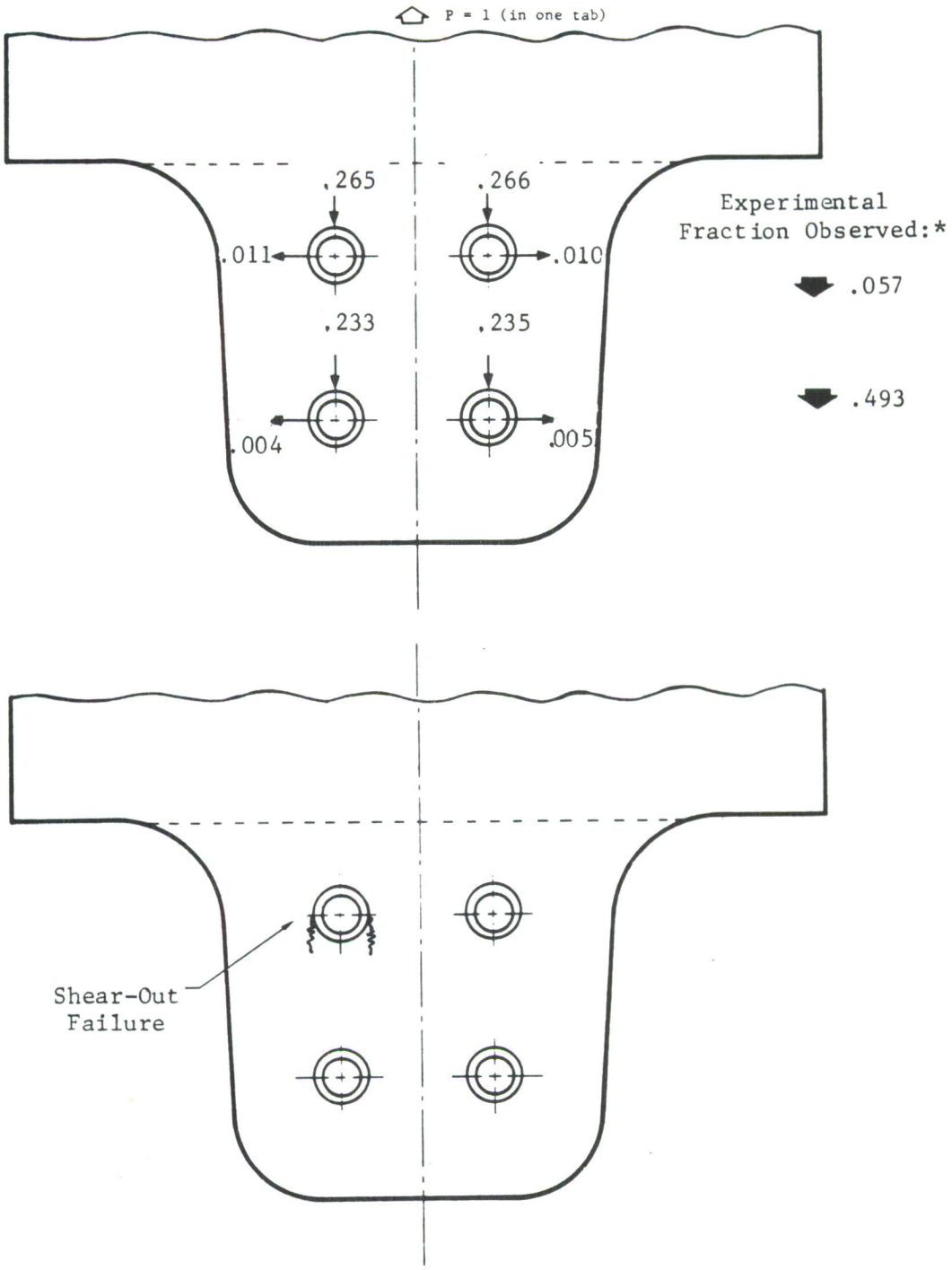

*Strain Gage Data

Figure 32. Load Distribution Among Fasteners, Failure Location and Failure Mode in the Graphite/Epoxy Tabs.

distribution between the top and second rows of fasteners (53.1% and 46.8%, respectively) was somewhat greater than the mearured values (50.7% and 49.3%) determined by the strain gage data. The predicted failure site (critical location) is in agreement with experimental observation (Reference 2).

Figure 33 presents the analytically predicted element load levels to precipitate net section, bearing and shear-out modes of failure at the various fastener locations. From the test results in Reference 2, the bearing strength for the laminate layup (60/26/14 percent of 0 /+-45 /90 plies) at the failure site may be assumed to be approximately 140 ksi, for protruding head fasteners, under room temperature dry conditions. Using this bearing strength and the load distribution in Figure 33, the element load corresponding to bearing failure in the top row of fasteners (preliminary design assumption) may be computed to be 123 kips. This agrees well with the predicted value of 127 kips (see Figure 33). However, this load level is higher than the element failure load corresponding to other failure modes originating from the top row of fasteners (see Figure 33).

Based on SAMCJ computations (Figure 33), element failure is predicted to occur at 98.0 kips, at the top left fastener location, in a shear-out mode. This corresponds to the lowest among the element load levels in Figure 33, corresponding to three assumed failure modes at every fastener location.

SAMCJ predictions also indicate that a net section failure across the top row of fasteners will occur at only a slightly higher load level. The observed failure mode, however, was severe damage around the fastener hole, introduced by the tilting of the countersunk fasteners (see Figures 26 and 27). This includes some amount of shear-out and local bearing, and severe delaminations around the fastener hole boundaries (see Figures 26 and 27). Since SAMCJ cannot account for the severe

local three-dimensional stress state introduced by the countersunk fastener, the predicted failure mode (shear-out) does not correlate well with the observed combined failure mode (partial shear-out, local bearing, and severe delaminations). An improvement of the fastener analysis segment of the SAMCJ code, to account for countersunk fastener geometry, must be complemented by the addition of a delamination predictive capability, to accurately predict the observed (complex) combined failure mode in the test element.

The analytically predicted element failure load of 98.0 kips is 7% larger than the measured value of 91.8 kips. Two factors contribute to this non-conservative prediction: (1) SAMCJ cannot accurately account for countersunk fastener effects; and (2) the failure criteria in SAMCJ do not account for delaminations that are introduced by the "digging in" of the countersunk fastener head (see Figures 26 and 27). Nevertheless, SAMCJ predicts the element tensile strength within 7% of the measured value, using the same material properties and failure parameters that were used in Reference 4.

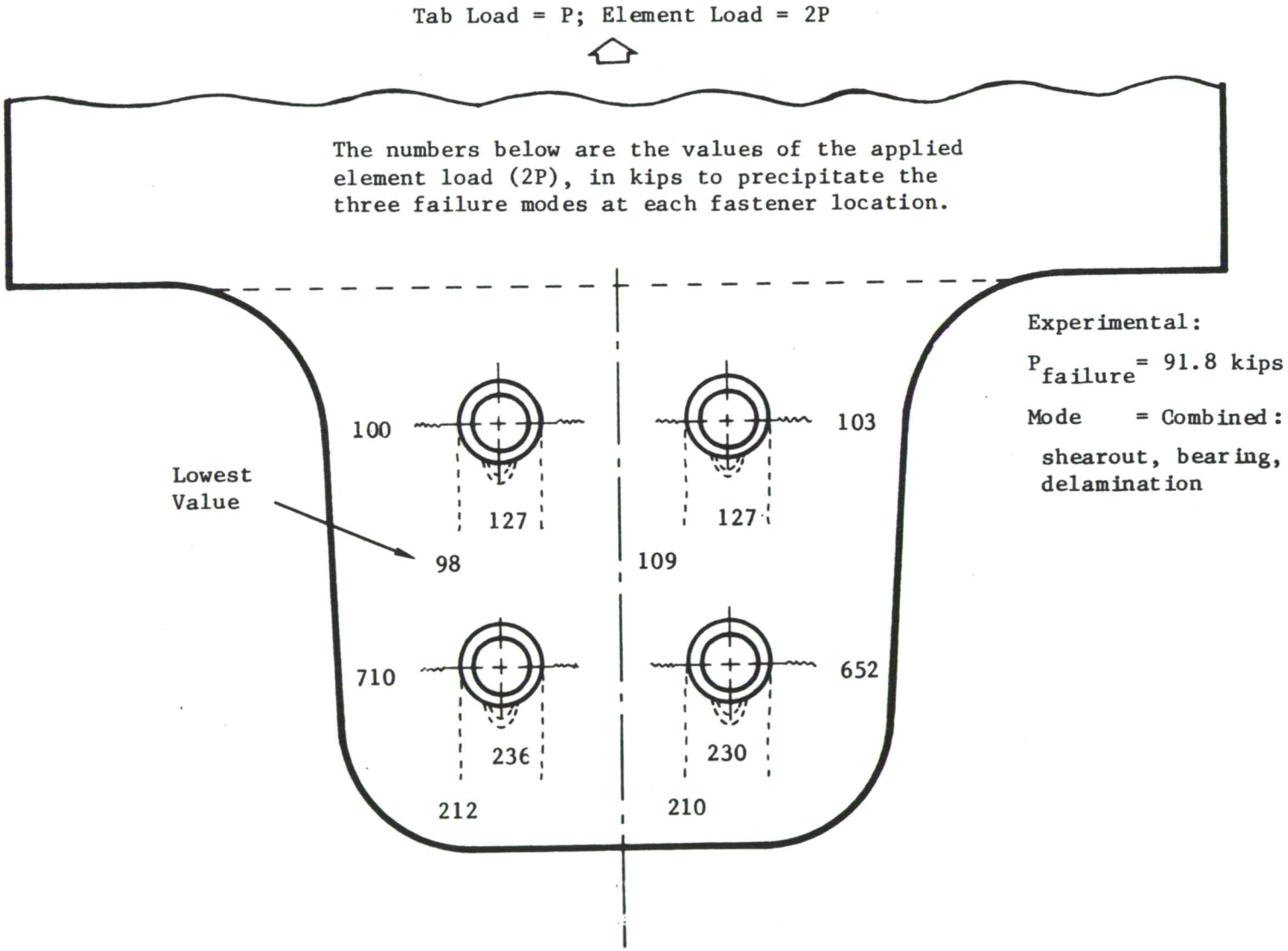

Figure 33. Analytically Predicted Element Load Levels to Percipitate Net Section, Bearing and Shear-Out Modes of Tab Failure at Each Fastener Location.

SECTION 5

CONCLUSIONS

Two elements were designed, fabricated and tested, to evaluate a direct bolting concept as an alternative to the existing F/A-18A vertical tail-to-fuselage attachment concept. The design of the element was based on an approximate analysis and a design ultimate load of 70.2 kips obtained from the F/A-18A empennage stress analysis report. Details of two elements were fabricated and assembled in accordance with design-generated drawings. The graphite/epoxy skins of the elements extended to the tab region that was directly bolted to the representative fuselage attachment fixture.

The two elements were initially subjected to two lifetimes of a representative tension-dominated F/A-18A vertical tail spectrum loading. The maximum spectrum load was the design limit load (46.8 kips) for the first lifetime, and the design ultimate load (70.2 kips) for the second lifetime. The imposed spectrum was significantly more severe than the actual F/A-18A vertical tail design spectrum load. The elements survived these fatigue loads without any indication of failure. Subsequently, they were subjected to static tensile loading to measure their residual strengths (89.9 and 91.8 kips for the two elements). Both the elements exhibited residual strengths that exceeded the design ultimate values by 28 to 31%.

The elements were analyzed using the SAMCJ computer code developed in this Northrop/AFWAL program. Since SAMCJ cannot accurately account for countersunk fastener effects, an equivalent (average diameter) protruding head fastener was assumed in the analysis. SAMCJ assumes three major laminate level failure modes at every fastener location (net section,

shear-out and bearing), and is incapable of predicting delaminations. The analytically predicted shear-out mode of failure was part of the observed combined failure mode (severe delaminations, local bearing and partial shear-out). Despite the mentioned limitations, SAMCJ predicted the element strength within 7% of the measured value, and accurately established the margin of safety in the preliminary element design.

The success of this Northrop/AFWAL program task added comfort to the design of an identical bolted joint concept at the subcomponent level in an ongoing Northrop/NADC program (Reference 7). It also established the adequacy of the SAMCJ computer code for predicting the strength of bolted joints in composite structures.

REFERENCES

1. Ramkumar, R. L., et al., "Strength Analysis of Composite and Metallic Plates Bolted Together By A Single Fastener," AFWAL-TR-85-3064, August 1985.

2. Ramkumar, R. L. and Tossavainen, E., "Bolted Joints in Composite Structures: Design, Analysis and Verification; Task I Test Results," AFWAL-TR-84-3047, August 1984.

3. Ramkumar, R. L., Saether, E. S. and Appa, K., "Strength Analysis of Laminated and Metallic Plates Bolted Together by Many Fasteners," AFWAL-TR-86-3034, July 1986.

4. Ramkumar, R. L. and Tossavainen, E., "Bolted Joints in Composite Structures: Design, Analysis and Verification; Task II Test Results," AFWAL-TR-85-3065, August 1985.

5. Ramkumar, R. L., et al., "Design Guide for Bolted Joints in Composite Structures," AFWAL-TR-86-3035, July 1986.

6. Kong, S. J., "Conceptual Design of a High Load Transfer Mechanical Attachment for Tail Structures," NADC-81216-60, August 1981.

7. Averill, S. W. and Zamani, H. R., "Development of High Load Joints and Attachments for Composite Structure," NADC-81220-60, August 1983.

8. Hilker, W. R., "F-18 Empennage Stress Analysis; Volume II (Vertical Tail and Rudder), "McDonnell Douglas Report MDC A5164, July 1978.

9. Garbo, S. P. and Ogonowski, J. M., "Effect of Variances and Manufacturing Tolerances on the Design Strength and Life of Mechanically Fastened Composite Joints," Volume 1, AFWAL-TR-81-3041, April 1981.

☆ U.S. GOVERNMENT PRINTING OFFICE: 1986 — 748-061/60563